

Answer to Referee Comment 1

S. Johansson et al.

September 22, 2020

We thank Michelle Santee for her thorough and very valuable comments and suggestions. We changed all minor language and wording corrections according to her suggestions without listing all of the changes in this answer. Instead, a latexdiff document that tracks all changes made in the revised manuscript is provided in the author's response file.

To our knowledge, Copernicus will have the manuscript copy-edited by a professional writer in case of acceptance and before publication in ACP. In addition, translation services at our institution (KIT) checked the language of the revised manuscript.

Our answers are given below. The original referee comment is repeated in **bold**, changes in the manuscript text are printed in *italics*.

P1, L16-17: It is not clear to me what the assertion that the models reproduce the large-scale structures of the pollutant distributions “if the convective influence on the measured air masses is captured by the meteorological fields used by these simulations” is based on, since this study does nothing to demonstrate that the models capture convective influence well, and in fact numerous prior studies have shown that they do not. Perhaps the large-scale trace gas distributions are controlled mainly by the large-scale circulation, which global models do simulate reasonably well.

We agree with the referee that we have not unambiguously demonstrated the influence of convective events to be responsible for the disagreement between models and GLORIA observations. Given the changes in the main part of the manuscript, we changed this part of the abstract to: *It is shown that these simulation results are able to reproduce large scale structures of the pollution trace gas distributions for one part of the flight, while the other part of*

the flight reveals large discrepancies between models and measurement. These discrepancies possibly result from convective events that are not resolved or parameterized in the models, uncertainties in the emissions of source gases, and uncertainties in the rate constants of chemical reactions.

P2, L4: The manuscript by Basha et al. (2019) has been rejected and should not be cited.

We thank the referee for pointing that out! We missed to check this reference before the submission of the manuscript.

P2, L7-8: Some references for the sentence about airborne in situ measurements inside the AMA would be appropriate.

We added the Bourtsoukidis et al., 2017 (10.5194/amt-10-5089-2017) and Gottschaldt et al., 2018 (10.5194/acp-18-5655-2018) references. Because both references (and other references we know) only describe measurements of air masses of the AMA edge outflow, we rephrased to: *Airborne in-situ observations of air masses belonging to the AMA are extremely sparse and often sample only filaments, border areas, or outflow of the AMA (e.g., Bourtsoukidis et al., 2017, Gottschaldt et al., 2018.)*

P2, L10-23: This paragraph as a whole is rather disjoint, with multiple independent thoughts assembled together with no thread connecting them. The last two sentences in particular seem out of place and do not follow from previous lines, and it's not clear why the last one begins with "However". I suggest rewriting to improve the cohesion and flow.

According to the comments of both referees, we reformulated and restructured this paragraph into two paragraphs: The second paragraph of the introduction now mentions studies about the transport in the ASM, focusing on open issues of vertical transport. The third paragraph of the introduction now summarizes studies of pollution trace gas measurements (and their implications) for the ASM UTLS.

P3, L30: This is a very abrupt transition to tropospheric ozone; it would be better to say something about background values of tropospheric ozone, and possibly its sources as well, before talking about the magnitude of enhancements.

We added typical O₃ VMRs in the ASM and restructured the paragraph, so

that the sources are discussed before the magnitude of enhancements.

P4, L4-5: Numerous papers (some of which are referenced elsewhere in this manuscript) have discussed the low abundances of ozone inside the AMA, so it is not appropriate to cite only a single paper for this point; at the very least an “e.g.” is needed here.

We added an “e.g.”, and Santee et al., 2017 and Brunamonti et al., 2018 as additional references.

P4, L10-11: This sentence is somewhat inaccurate. Ozone is typically low inside the AMA; the Park et al. papers cited here use low ozone abundances (along with enhanced CO) as a marker of tropospheric air trapped inside the AMA. Park et al. (and others) have used larger abundances of ozone as an indicator of the presence stratospheric air, but not “polluted air” as stated here. If the authors are referring to the findings of Gottschaldt et al. (2017), then that paper should be cited here. In addition: measurements of O₃ ... is → O₃ is.

We rephrased this sentence. In addition, we added the suggested reference: *Similarly to HNO₃, enhanced O₃, within the generally O₃ poor AMA upper tropospheric air, is either interpreted as indicator of stratospheric air (e.g., Park et al., 2007, 2008) or connected to uplift of O₃ precursor species of polluted air (Gottschaldt et al., 2017).*

P4, section 2.1.3: Typical background abundances of PAN should be stated here, as they are in the respective subsections for HNO₃ and O₃. This information is given in Section 3, but for completeness it should appear here as well.

According to the referee’s suggestion we added: *Typical background abundances of PAN in the upper troposphere are below 100 pptv (Glatthor et al., 2007).*

P4, L17-18: It is stated that photolysis plays a minor role, but according to Fadnavis et al. (ACP, 2015), photolysis is the dominant loss process for PAN in the UTLS. In addition, 250 K is not a higher altitude than 298 K.

Our original statement was meant for the whole troposphere. We added Fadnavis et al. (ACP, 2014) as reference for this sentence and formulated

more precisely: [...] and photolysis play a minor role for lower tropospheric altitudes (e.g., Fadnavis et al., 2014). In the upper troposphere instead, photolysis is the dominant loss process for PAN (e.g., Fadnavis et al., 2015). In addition, we clarified, that the numbers given are temperatures, not potential temperatures.

P4, section 2.1.4: It is even more critical to help readers by providing some idea of typical background values for acetylene since that information is not given in Section 3.

We added: *Typical background values for C₂H₂ are below 75 pptv (e.g., Xiao et al., 2007; Wiegele et al., 2012).*

P5, L13-14: Why is only a single research flight singled out for analysis in this study? Unless some explanation is given about why the data available from the other three flights are not considered, readers may draw their own inferences about their quality or consistency.

We added these sentences for explanation: *This research flight was selected for this work due to high flight altitudes and low cloud top altitudes within the AMA, which are both optimal measurement conditions for the infrared limb instrument GLORIA. This research flight was by far the best, due to the flight length allowing different air masses to be sampled and the low cloud top altitude.*

P7, L10-15: These sentences are poorly written and unclear. Was the extension of the MECCA model performed by the authors as part of this work, or by the EMAC team? Are the values quoted for the number of reactions, etc., for the “standard” MECCA submodel or the “extended” one?

Sorry for the confusion, we selected a more comprehensive chemistry setup as usual in our simulations. The MECCA submodel was not extended. We removed the word “standard”, because we do not explain it in the text and changed the sentence accordingly: *The chemical setup of the chemistry submodel MECCA (Sander et al., 2011) was selected with focus on the simulation of PAN and tropospheric chemistry.*

P7, section 2.3.1: How are emissions prescribed in the EMAC runs done for this study? This information seems just as critical to me

as the details of the chemical submodel. In particular, if emissions were prescribed using RCP scenarios, which do not include specific events, such as major fires in any given year, then even specified-dynamics EMAC simulations cannot be expected to replicate the observations closely.

The referee is right, the emissions do not include the specific events of the year 2017. We use an emission scenario, which is quite common in the climate modeling community and currently, we do not have more recent emission data for the year 2017. We will express this more clearly in the paper. Nevertheless, we are convinced that the EMAC results should remain in the paper, because we think that simulation results based on these commonly used emission scenarios should be compared to measurements.

P7, section 2.3.2: Similarly, information about the emissions in CAMS also needs to be given.

We added: *Anthropogenic emissions are prescribed by MACCity (MACC/CityZEN; Granier et al., 2011), biogenic emissions by MEGAN2.1 (Model of Emissions of Gases and Aerosols from Nature; Guenther et al., 2012), and biomass burning emissions by GFAS v1.2 (Global Fire Assimilation System; Kaiser et al., 2012).*

P7, L23-24: This sentence mentions a study evaluating the CAMS chemical reanalysis using aircraft measurements but provides no information about the results of those comparisons. Did Wang et al. (2020) find that CAMS fields match the measured species well or not? What are the implications for this work? In addition, the paper by Wang et al. has now been published, so the reference needs to be updated.

Thanks for reminding us of the updated Wang et al., 2020 paper. We added to the section: *Profiles of O₃, HNO₃, and PAN above Hawaii showed an agreement within the uncertainties of measurement and model. These agreements encourage the model evaluation of this study at altitudes of the upper troposphere in the ASM.*

P8, L9-10: Is this 3-h ERA5 product different from the one mentioned on P7, L28 with 1-h temporal resolution?

Both trajectory models (TRACZILLA and ATLAS) use the same ERA5 product, but ATLAS used a 3 h temporal resolution and a different spatial

grid. We changed the manuscript to: *Trajectories from the ATLAS model (Wohltmann et al., 2009) are driven by the same ECMWF ERA5 meteorological fields as TRACZILLA, but with a temporal resolution of 3 h and a horizontal resolution of $1.125^\circ \times 1.125^\circ$.*

P8, L22-26: The investigation described in these sentences is interesting, but the results reported here are vague and their implications for this study are unclear (and the last sentence in this paragraph could also be better composed). What exactly is meant by “major differences” and “minor influences”? This discussion should be more quantitative. Do the findings from these ATLAS and TRACZILLA tests have any implications for the results from EMAC, since those runs were driven with ERA-I?

We added an additional figure to the supplement (Suppl. Fig. 19) to exemplarily show the influence of the reanalyses, trajectory type, and diffusion on the trajectory paths and location of convective events. We now refer to this supplementary figure and rephrased these sentences. In addition, we now reference to this investigation in the discussion of possible improvements of the EMAC simulations: *In an analysis of the ATLAS trajectories, the influence of the usage of ERA5 or ERA-Interim as meteorological fields, the influence of applied vertical diffusion, and the influence of the usage of kinematic or diabatic trajectories was investigated (shown in the supplementary information). This analysis (and also similar analyses by Legras and Bucci (2019)) revealed that major differences occur between ATLAS trajectories that use ERA5 or ERA-Interim meteorological fields. These major differences are exemplarily visible in Supplementary Fig. 19, where trajectory paths and locations of convective events are considerably different between ERA-Interim and ERA5. Compared to these large discrepancies, differences in trajectory paths and locations of convective events due to the usage of kinematic or diabatic trajectories, or due to the application of vertical diffusion are small.*

P8, section 2.3.5: It is necessary to provide information on the quality and resolution of the OMI tropospheric column NO₂ data, as well as a suitable reference for this specific product (beyond the general OMI instrument paper and the Krotkov (2013) citation, which is just for the L3 files and which is also incomplete).

We added: *The version 3 standard retrieval of tropospheric column NO₂ comes with a spatial resolution of $1.0^\circ \times 1.25^\circ$ (latitude \times longitude), and*

showed an overall agreement with other satellite and ground based measurements of NO₂ (Krotkov et al., 2017).

The Krotov (2013) citation was meant as a documentation of the data file we used for this work, which is encouraged to be used by ACP. Due to technical issues, the DOIs were not displayed in the bibliography, which is now fixed.

P9, L6-7: This wording is unclear. By “local enhancements up to 0.5 ppbv”, do the authors mean that the measured mixing ratios approach 0.5 ppbv, or that they are 0.5 ppbv larger than the regional background values (it looks like the latter to me). Some of these enhancements appear to be located at altitudes higher than 16 km. In fact, the particular structure noted at 4:00 UTC is at more like 16.5 km.

We tried to formulate more precisely: *In the first part of the flight (until 4:45 UTC), also a local maximum of VMRs up to 1.0 ppbv is visible below the tropopause at altitudes between 15.5 km and 17 km (close to the red box in Fig. 2b).*

P9, L8: Why is the magenta box drawn so as to exclude the peak in this enhancement at 4:00 UTC, and also the higher values right at 16 km just before 4:15 UTC? If this enhanced structure is of interest for further analysis, I would think that it would be desirable to encompass the region of its strongest signature.

We added the (slightly adjusted) red box to the HNO₃ cross section plot and clarified: *This maximum is continued by enhancements noted at 16 km at 4:00 UTC moving down to 15 km at 4:15-4:50 UTC with VMRs up to 0.75 ppbv (marked with a magenta box). The shape and position of the red and magenta boxes are optimized for the pollution trace gases PAN and C₂H₂ discussed later in this section to have a local maximum in the red and a local minimum in the magenta box. Thus, these boxes do not exactly match the structure in HNO₃. In addition, Höpfner et al. (2019) reported enhanced ammonium nitrate abundances in the red air masses, and a local minimum of ammonium nitrate in the magenta box. Given these different pollution trace gas and aerosol concentrations in the red and magenta boxes, it is assumed that these air masses have different origin, even though the structure in HNO₃ appears to be connected.*

The adjustment of the red box induced changes in Sec. 4.

P9, L14-15: It would be helpful if the colored boxes on Figure 2 were also overlaid on Supplementary Figures 2, 4, 6, 8, and 10. We updated these Supplementary Figures according to the referee's suggestion. In addition, we refined the statement about the O₃ error within the purple box.

P11, L5-9: I'm wondering why the authors have chosen not to highlight the region with the minimum in HCOOH where PAN and C₂H₂ are present in its own colored box. Considerable discussion is devoted to this part of the flight, possibly more than for some of the regions that are enclosed within boxes.

We added a green box to highlight this minimum in HCOOH. We know, that the green color might be difficult to see on top of the cross section, but with the white border all colored boxes have, it should be possible. We decided for this color because it is also easy to separate from the other colors in the written discussion later in the manuscript.

Figure 2: It would be extremely helpful to the reader to: (1) enlarge the major tick marks on both x and y-axes, (2) add minor tick marks, and (3) include tick marks on the right-hand y-axis and the top x-axis. Without them, it is very difficult to judge the values quoted in the text

We changed the figure (and similar figures later in the manuscript) according to the suggestions.

The colored boxes on both the maps and the curtain plots are a little hard to see, as is the green line marking the tropopause. Perhaps it would help to make these lines a bit thicker.

We increased line thicknesses according to the suggestions. In line with suggestions from the second referee, we also changed the color of the 380 K tropopause line to dark gray.

P12, L11: Although the overlaid boxes in Figure 3 facilitate comparison with Figure 2, the authors should consider adding an altitude scale on the right-hand y-axis of the panels as well. It would also be helpful to state the approximate pressure level corresponding to 15 km in this line.

We followed the suggestion of the referee and added an additional y-axis with

an approximation of altitude to the plots. In addition, we also mentioned the corresponding pressures in the text.

P12, L16-19: My apologies, but I am missing something here. I don't quite understand how the densities of convective events discussed in this paragraph relate to the convection probabilities shown in Figure 3 and discussed in the previous paragraph (which are an order of magnitude larger). Please clarify the relationship between these two quantities.

We have substantially rephrased the complete paragraph to make more clear what is shown in Figures 3 and 4 (also in response to your comment on P12, L20). The text was confusing and did not contain sufficient information for the reader to understand the method and the figures. In addition, there was a factual error in the text which increased the confusion: "the smallest bordered regions include at least 0.1% of convective events" should have been "the outermost contours include at least 0.1% (per square degree) of convective events" (i.e. just the opposite of what was written). We have also made more clear now that the unit of the fractions shown in Figure 4 is "percent per square degree", i.e. the quantity shown is a fraction per area and not just a fraction.

P12, L20: I'm confused here too – why would it necessarily be the case that "larger regions contain accordingly a larger fraction"? A large region encompassed by a single colored contour but no inner contours would still have convective densities between 0.1% and 1.0%, no matter its size. Unless an inner contour is present, the fraction does not reach 1.0%. In addition, I have looked closely at Figure 4, and I am not convinced that any of the outlined regions contain the innermost contour representing 10%, except for one orange region in the TRACZILLA panel. Perhaps the rarity of that occurrence should be pointed out.

The statement was incorrect and we have rephrased the paragraph (see also reply to P12, L16-19).

P14, L8-9: The flow in this paragraph needs to be improved. The sentence about the small fraction of trajectories experiencing convection in the 5 days leading up to the measurement is ambiguous; it immediately follows a sentence on the magenta region and thus

appears to be about that area, but in fact I think it is referring to the red region. This should be clarified.

We removed the reference to the magenta region, which is not needed in this paragraph. We apologize for the confusion.

P14, L10-12: The writing in these lines is very unclear. Assuming that I have interpreted them correctly, I suggest instead: “For most regions marked red, only the 0.1% contours are present; thus convective influence along the trajectories was weak. However, most regions marked red in northeastern China lie close to areas with enhanced NO₂, so these regions may possibly have contributed to the measured enhanced pollution trace gases.”

We changed the manuscript in line with the referee’s suggestion. In addition, we changed the order of words in the first sentence to make cause and effect more clear: Because convective influence was weak, only the 0.1 percent per square degree contour is present.

P14, L13-14: Again, I am confused about how the 30% value quoted here for the red regions can be reconciled with the 1% contour outlining those regions in Figure 4. The sentence in these lines is quite unclear. I’m also confused about exactly what is being shown in Supplementary Figure 12. As I understand it, the trajectories are launched from the GLORIA measurement locations, which in many/most cases are not characterized by ongoing convection. However, although the caption to Figure S12 is unclear, particularly the description of panel (c), it seems to suggest that a convective event was occurring at the time the trajectories were launched, and that 30% of those back trajectories had experienced convection leading up to that point. Please clarify.

We have substantially rephrased the text and the caption in the supplement. In particular, we did not want to suggest that a convective event was occurring at the time the trajectories were launched, which is not the case. We changed the text in the manuscript to: *For the ATLAS model, it is shown in Supplementary Fig. 12 that for the red region, less than 30% of all started trajectories experienced a convective event within 10 days before the measurement, showing the weak convective influence.*

In addition, we changed the caption of Fig. S12 to: *In b) and c), dots mark the location of all convective events experienced by backward trajectories starting*

in the red region (with the convection scheme switched on). b) is color-coded with the time difference between the convective event and the time of measurement, and c) is color-coded with the percentage of the other backward trajectories that already had experienced convection when the trajectory represented by the dot went into convection.

P14, L15-16: The magenta box is not shown on Fig. 2i, j, nor was a minimum in HCOOH in this region discussed (P11, L1-17). If anything, HCOOH looks slightly high in that area. I assume that “close to the red maximum” is referring to the pollutant enhancements in the red box?

We thank the referee for pointing that out! HCOOH appears in that list by mistake. We removed it from this paragraph. We changed the formulation “close to the red maximum” to *close to the maximum of the pollutant species marked with the red box.*

P14, L19-20: This sentence is badly written and hard to read. I suggest instead: “However, in this case, it is likely that convection in the regions above the South China and Philippine Seas brought up clean maritime air.” But perhaps I have not understood this sentence. I can see that convective transport of clean maritime air could produce a local minimum in the pollutants, but how could it have led to enhanced HNO₃ in this region?

We changed the sentence according to the referee’s suggestion. In addition, for the explanation of the enhanced HNO₃, we add: *Enhanced HNO₃ concentrations within these air masses possibly result from reaction of lightning NO_x with OH to HNO₃ (see e.g., Schuhmann et al., 2007).*

We compared typical lifetimes of NO_x in the upper troposphere (4-7 days according to Schumann et al., 2007; 10.5194/acp-7-3823-2007) with the time since the convective event above the South China and Philippine Seas for the magenta air masses (3-5 days; see Suppl. Tab. 1). Together with observations of several ppbv of lightning NO_x (Schuhmann et al., 2007), and HNO₃ as main sink of lightning NO_x, we consider this to be the most likely origin of the enhanced HNO₃ concentrations. In addition, we added in response to the referee’s comment on “P9, L8” a comment on the structure of HNO₃ in the first part of the flight.

P14, L28-29: This sentence is unclear. More plausible than what?

More likely than what?

We rephrased this sentence to: *This corresponds to the orange region in India with enhanced NO₂ columns.*

Other information in the original sentence was redundant to preceding sentences.

P15, L3-4: Why would bringing up relatively pristine marine boundary layer air lead to a local enhancement in ozone?

We added an interpretation of this result from the trajectory analysis: *These areas marked by the trajectories show low OMI NO₂ and indicate relatively clean boundary layer air, which cannot explain the measured local enhancement of O₃. This suggests that the measured local maximum of O₃ is of other than convective origin; possibly, the measured maximum is a pollution remainder transported for more than 10 days, or an intrusion of stratospheric air.*

P15, L6-7: I do not follow the logic here. The relevant sentence in Section 3 “suggests that these air masses are older than a few days (lifetime of HCOOH), but younger than 2 weeks (lifetime of C₂H₂)”. How does that lead to the statement here that “convection 10 days before the measurement only had a minor influence” – that is, where does the value of 10 days come from? Perhaps the authors mean “convection any time in the last two weeks”?

This sentence was confusing and we changed it to: *In Sec. 3, it is suggested that these air masses are transported for more than a few days, but for less than two weeks. For this reason, it is not expected to see strong convective influence in the trajectories a few days prior to the measurement.*

P15, L15: I’m not sure what the take-away message for the reader is. Does the fact that both models seem to identify source regions that are less “plausible” call into question the entire source attribution analysis? Are these regions really less plausible as source regions because they are characterized by low OMI tropospheric column NO₂? As mentioned in connection with Section 2.3.5, some discussion of the reliability and sensitivity of these OMI data is needed. Moreover, can it necessarily be assumed that tropospheric column NO₂ is a robust proxy that reflects *all* possible sources for these NMVOCs? In particular, according to Section

2.1.5, formic acid arises in part from biogenic emissions. Would those be captured in the NO₂ measurements? Some further discussion is warranted here.

We rephrased and extended the last paragraph of this section, after a summary of air mass origins (as asked for by referee 2): *The comparison of ATLAS and TRACZILLA calculations of convective origin of the measured pollution species shows that there are few differences between these model results. Both models give results for the source regions and convective age of air that are broadly consistent with the measurements. Due to the numerous uncertainties, there are, however, also some results which seem to be less plausible. However, OMI NO₂, which is shown as proxy for boundary layer pollution, does not account for biogenic sources and is shown as average over 14 days prior to the measurement (see Sec. 2.4). Due to these limitations, additional pollution sources may have been overlooked in this analysis. Still, similar origins of highly polluted air masses, indicated by two independent backward trajectory models, agree with enhanced surface pollution, measured by OMI. This agreement within the anticipated accuracy of the two backward trajectory models suggests that both models use reliable schemes for convection detection.*

P15, L25-26: The EMAC HNO₃ mixing ratios at the tropopause look quite a bit smaller than 0.75 ppbv to me. In addition, the writing in this sentence is very awkward; I suggest rewriting as: “. . . flight; they decrease to values of 0.75 ppbv at the tropopause. Simulated maximum stratospheric values are not always as high as those measured, but they agree to within”

This is correct! We checked again in the data and at the tropopause in the second part of the flight, HNO₃ actually goes down to 0.5 ppbv. We changed the formulation according to the referee’s suggestion.

P15, L31-P16, L2: The authors posit that the diagonal feature in the HNO₃ field simulated by EMAC may originate from reactions with NO₂, and the tone of the discussion seems to suggest that this may be a model artifact, especially in the latter portion of the flight. But they have made no attempt, here or in the previous section, to account for the similar feature seen in the GLORIA measurements in the first half of the flight. What is the explanation for the observed structure in HNO₃?

We added a short discussion about this diagonal feature in HNO_3 : *The difference in this diagonal structure between GLORIA and EMAC in the second part of the flight may result from a spatial displacement of the whole structure in the model, which is, however, unlikely due to the agreement of this HNO_3 structure in the first part of the flight, and due to the agreement of structures in pollution trace gases in the second part of the flight (see below). It is more likely that EMAC overestimates the production of or underestimates the loss of HNO_3 here at altitudes below 14 km.*

P16, L5: It would be appropriate to include a reference for the CAMS assimilation of O_3 .

We added the Inness et al., 2015 reference (10.5194/acp-15-5275-2015). It describes the assimilation scheme for the MACC data product, a precursor of CAMS.

P17, L15: In addition to pointing out that the EMAC C_2H_2 enhancement is in the same geolocation as the measured enhancement, it would be good to note that the simulated enhancement is much weaker and less extensive than the measured enhancement; it would also be helpful to add “(cyan box)” here.

We changed the sentence to: *In the second part of the flight, again a very small enhancement at the tropopause at 6:00 UTC (cyan box) is visible in EMAC, which is at the same geolocation as the enhancement in the measurements, but much weaker and less extensive.*

P17, L12-15: A point that is missing from the C_2H_2 discussion is the fact that EMAC completely fails to simulate the maxima in the red and orange boxes and the minimum in the magenta box, even in a relative sense.

We added the sentence: *Measured maxima of C_2H_2 are not reproduced by the EMAC model.*

P17, L25-26: The authors state that their results indicate that the meteorological fields used to prescribe transport in the simulations do not include processes relevant for the observed situation. I presume that they are referring to deep convection, which is not resolved by the reanalyses, but that should be clarified. I am wondering, however, why this would be a factor only for the first part

of the flight (which the sentence in question is about). According to Figure 3, as well as much of the discussion over the preceding pages of the manuscript, the second half of the flight was influenced by convection up to 150 hPa to a similar degree.

We agree that the paragraph this sentence originates from was badly formulated. We restructured the whole paragraph and tried to be more precisely.

P18, L57: The writing in these sentences is clumsy. Moreover, I'm afraid that I don't follow the logic of the arguments. First, as mentioned in an earlier comment, both portions of the flight are characterized by high convection probabilities up to 150 hPa, so for that reason alone it doesn't make sense to focus only on the second half. Second, the authors appear to be saying that *because* the first part of the flight is strongly influenced by convection, the simulated results would not be affected by increased emissions. But that seems backwards to me – in the absence of convection, the strength of the surface emissions would be of little consequence. This discussion needs to be clarified.

Also based on the feedback from referee 2, we decided to move the sensitivity test that is discussed in Sec. 6 to the Supplementary Materials. We only provide a short summary of the quite lengthy discussion of Sec. 6 at the end of Sec. 5. For this reason, the sentences that are addressed by this comment are no longer part of the revised manuscript.

P19, L6-8: I'm not sure that it is true that GLORIA did not observe the slight enhancement in HCOOH at 6:00 UTC and 16 km. There may be a faint hint of this structure in the data. Perhaps this feature should have been introduced earlier in the discussion, e.g., P17, L16-22.

We added to Sec. 5: *In the averaged GLORIA cross sections, a small local maximum of 60 pptv is visible after 6:00 UTC, which coincides with the small enhancement in EMAC.*

However, the sentences that are addressed by this comment are no longer part of the revised manuscript.

P19, L10-14: Of course, although the increased emissions led to larger maximum values of PAN that matched the observed peak abundances better, they did nothing to improve the structure of

the simulated field. I do not think that this is an unanticipated result. I would have expected background abundances of these tropospheric tracers to rise along with peak abundances in the increased-emissions scenario. So I am slightly puzzled by the discussion in these lines, which focuses on the impact of vertical resolution on the modeled fields. Its placement in this paragraph seems to imply that the smoothing effect of the coarser resolution of EMAC, which blunts peak abundances and blurs or erases fine-scale features, is somehow responsible for the background values of PAN being too high in this sensitivity test. In fact, I think that the resolution issue is just as relevant for the baseline model run, in which background abundances were also overestimated, and it would be more appropriate to move the discussion about it to Section 5.

We added the discussion of overestimated background VMRs and the resolution issue to Sec. 5. However, the sentences that are addressed by this comment are no longer part of the revised manuscript.

P19, L16: The possibility that model/measurement discrepancies may be partly attributable to emission sources not represented in the inventory used in these EMAC runs is mentioned. As I noted in connection with Section 2.3.1, which emission inventories were used in these simulations is a critical piece of information that has been omitted from the manuscript.

We added the missing information to Section 2.3.1. However, the sentences that are addressed by this comment are no longer part of the revised manuscript.

P19, L18: That the meteorological reanalyses do not resolve local deep convection is a wellknown issue that is presented here as a finding of this study. In addition, another aspect (besides the reanalyses) that does not appear to have been considered by the authors is the convective parameterization being used for these EMAC simulations. The choice of which convective parameterization is used has been shown to have a substantial impact on modeled trace gas distributions.

For convection, we use the parameterization introduced by Tiedtke (1989) with modifications by Nordeng (1994) as described in Tost et al. (2006). So

far, this has been the best choice for our EMAC simulations. We will add this information to the EMAC description.

In addition, in the discussion of Sec. 5, we now refer to the large uncertainties of convection parameterizations used by EMAC, as reported by Tost et al. (2006).

P19, L23: In my opinion, the statement that this study discusses “the first measurements of HNO₃, O₃, PAN, C₂H₂, and HCOOH in the center of the AMA UTLS” is too broad. While that may be true for some species of the species listed, it is not true for all of them. This statement should be qualified in some way, e.g.: first airborne measurements, or first measurements by GLORIA.

We formulated more precisely: *This study discusses the first simultaneous airborne measurements of HNO₃, O₃, PAN, C₂H₂, and HCOOH in high spatial resolution in the center of the AMA UTLS.*

P19, L29-30: This study is not the first to show that PAN is efficiently transported to the UTLS by deep convection, as is implied by the wording in these lines.

We changed the sentence to: *These measurements and their analysis confirm that PAN, a precursor of O₃, is efficiently transported upwards by convection, and transported for a longer time in the tropopause region, as shown earlier by Glatthor et al. (2007), Fadnavis et al. (2015), and Ungermann et al. (2016).*

P20, L6-8: Some of the discussion here is appearing for the first time in this manuscript. I do not think that it is appropriate to introduce new concepts in a section entitled “Conclusions”.

We moved this sentence to Sec. 3 and referenced this thought only briefly here.

P20, L23-25: As noted earlier, the fact that EMAC overestimates tropospheric background mixing ratios is not unique to the increased-emissions scenario – it was also the case for the baseline run, and increased emissions are expected to affect background as well as peak abundances. The same comment regarding vertical resolution applies here as well.

We added the aspects of overestimated background VMRs and resolution to the discussion of the baseline run, while the original sentence has been

omitted in the revision of the manuscript.

P20, L31-34: These sentences are poorly written. “enhancements” are not transported upward – pollution is transported upward, leading to enhancements in the UTL. Likewise, a “region” is not transported “around the tropopause” – the measured air masses in that region are transported. And I’m not sure what is meant by “around the tropopause”.

We changed the sentence to: *Some pollutants have been transported into the upper troposphere by convection within days before the measurements, while one part of the observed air masses remained at UTL altitudes for a longer time.*

Answer to Referee Comment 2

S. Johansson et al.

September 22, 2020

We thank the referee for valuable comments and suggestions. We changed all minor language and wording corrections according to the suggestions without listing all of the changes in this answer. Instead, a latexdiff document that tracks all changes made in the revised manuscript is provided in the author's response file.

To our knowledge, Copernicus will have the manuscript copy-edited by a professional writer in case of acceptance and before publication in ACP. In addition, translation services at our institution (KIT) checked the language of the revised manuscript.

Our answers are given below. The original referee comment is repeated in **bold**, changes in the manuscript text are printed in *italics*.

P2, L16-17, what's the name of the aircraft campaign?

We added the name of the Earth System Model Validation campaign to the manuscript. For the next sentence, we also mention now the Oxidation Mechanism Observations campaign.

P2, L22-24. The logical connections of these two sentences and the previous section seems to be amiss. What's the relationship between radiative heating rates and transport in reanalyses with trace gases? Observations are sparse, so what? How do observations help? The last sentence in the next paragraph (atmospheric chemistry models ...) is out of place. It fits much better in this paragraph, instead.

According to the comments of both referees, we reformulated and restructured this paragraph into two paragraphs: The second paragraph of the introduction now mentions studies about the transport in the ASM, focusing

on open issues of vertical transport. The third paragraph of the introduction now summarizes studies of pollution trace gas measurements (and their implications) in the ASM.

In addition, we removed the “atmospheric chemistry models” sentence from the next paragraph.

P2, L24-28. These three sentences seem to repeat themselves in various ways. It can be easily condensed into a single sentence but capture all essential elements. Please revise.

We agree that the third sentence did not provide much new information. It would be possible to also merge the first two sentences, but in our opinion, this would not improve readability. We propose to change the first four sentences to these two sentences: *The first observations of the upper tropospheric chemical composition in the region of the ASM in high vertical resolution have been obtained during the high-altitude airborne StratoClim (Stratospheric and upper tropospheric processes for better climate predictions) campaign. This study presents a unique data set of pollution trace gases, in particular non-methane volatile organic compounds (NMVOCs) obtained with the Gimballed Limb Observer for Radiance Imaging of the Atmosphere (GLORIA) during this StratoClim campaign based in Kathmandu, Nepal, 2017.*

P3, L1. Which two models? EMAC and CAMS? Please specify. And I am sure this is not the “first evaluation” of these two atmospheric chemistry models.

We changed the sentence to: *Second, a first evaluation in high spatial resolution in the ASM UTLS of the atmospheric chemistry models EMAC and CAMS is provided [...]*

P3, L30. WMO, 2019 – > This one is actually “WMO, 2018”

You are right that the WMO report referenced here is named “Scientific assessment of ozone depletion: 2018”, but it was published in January 2019 (see <https://www.esrl.noaa.gov/csl/assessments/ozone/2018/downloads/2018OzoneAssessment.pdf>, page ii), which makes it a publication of the year 2019. However, in case of publication in ACP, Copernicus Publications will adjust the references according to their standards.

P4, L1. Catalytic reactions with nitrogen oxides is a sink of ozone in the stratosphere and to some extent in the upper troposphere.

Primary sources of ozone in the troposphere is in situ production of NO_x + HO_x, and NO_x + peroxide radicals from VOC oxidation, hence indicator of polluted air masses.

We refined our explanation of tropospheric ozone sources according to your comment and restructured the section according to the comment in Michelle Santee's review. In addition, we added reactions with NO_x to the loss processes (Bozem et al., 2007; 10.5194/acp-17-10565-2017) and mentioned lightning as a source of NO_x.

P4, L27. Maximum tropospheric mixing ratios of a few ppt for C₂H₂? Are you sure it is not a few ppb?? Check Xiao et al., (2007).

Yes, you are right, that was a typo.

P7, L14. Can you describe what are the NMVOC emission sources used in EMAC? When you say 50% and 100% additional emissions, do you mean from all emission sources, e.g. biomass burning, bio-fuel, fossil fuel, etc., and globally or just over Asia?

There are anthropogenic emissions sources from biomass burning, agricultural waste burning, fossil fuels, ship, road and aircraft emissions, as well as biogenic emissions. We included this in the paper. The emissions are from MACCity, ACCMIP and RCP6.0. In our sensitivity studies, we added 50% or 100%, respectively to all NMVOC emission sources globally. We explain this now also in the description of the EMAC model simulations.

P8, L3-4. I find this sentence very awkward, with no clear description of what was actually done.

We changed this sentence to: *A trajectory is considered to be influenced by convection if it encounters a convective cloud during its advection, with a pressure higher than the cloud top pressure (similarly done by Tissier et al., 2016). The location of cloud encounter is then identified as a convective source.*

P7-8. In sections 2.3, could you also provide the details on which year, time period of the model simulations that were conducted?

For EMAC, it is already mentioned at the end of Sec. 2.3.1 that all model runs were initialized on 1 May 2017. The CAMS reanalysis is an operational data product from ECMWF and similarly to other reanalyses continuously

updated. We added to the manuscript: *CAMS reanalysis data is available for the time between 2003 and 2018.*

Both backward trajectory models simulate the time before the measurement. For TRACZILLA, it is already stated in Sec. 2.3.3 that they are simulated for one month before the measurement. For ATLAS, we added: *Trajectories are calculated for 30 days prior to the measurement.*

P8. Section 2.3.5 is out of place. This is observations and it should be listed in Section 2.1 or Section 2.2, not in the modeling subsection.

Thanks for pointing that out! We modified the structure so that the OMI part is now in its own subsection.

P9, L3 and Figure 2. I think it is more accurate to say these are colored boxes are “air masses” of interest, rather than “regions” of interest. Also in figure 2 caption, add “shows” after “the green line”. I find the green line very hard to see. A thick solid dark gray line would be much better. It also distinguishes its functionality from the color boxes.

We agree that the formulation “air masses of interest” is more accurate and changed this term throughout the manuscript. We also followed your suggestion to change the color of the 380 K tropopause to dark gray and thickened the line.

P10, Figure 2. I find all panels very noisy, which is not surprising due to the large errors in GLORIA measurements as listed in Table 1. I would suggest average the measurement samples to larger temporal and vertical bins. This way you can average down the noise and illustrate the discussed features much better. In the present form, these features are barely distinctive from the surrounding background air masses. This is particularly problematic from C2H2 and HCOOH.

One goal of this manuscript is to publish the GLORIA data set for this StratoClim science flight, characterized by estimated error and vertical resolution. For this reason, we prefer to present the data in the full spatial resolution. Later in the manuscript, for comparisons with the EMAC and CAMS models, we horizontally average GLORIA profiles for a better comparison of the major structures. This averaging also reduces the noise error,

which is a large contribution but not the total estimated error (see Suppl. Figs. 1, 3, 5, 7, 9). The other major contribution to the total error is the pointing error, which is not a statistical error and is thus not reduced by averaging of profiles. Vertical averaging, as suggested by the referee, would make the vertical resolution, which is an important characteristic of the retrieval, very difficult to interpret by the reader. As a compromise to better illustrate the discussed features, we changed the colorbars to discrete values instead of a continuous color spectrum, which also reduces noisy structures that are in the order of magnitude of the total estimated errors.

P12, Figure 3 and the corresponding discussion. (a) In the text, the relevant discussion uses km as a unit while the y-axis only shows pressure. Please add the corresponding km on y-axis. (b) The cyan box in TRACZILLA show likely convective influences while ATLAS shows none. Why the two models are showing such different results? And how can the GLORIA measurements help in assessing which back trajectory model is more accurate. Also, overall, I can see TRACZILLA shows more convective influences than ATLAS. How can you assess which one is more accurate?

(a) We followed the suggestion of the referee and added an additional y-axis with an approximation of altitude to the plots. In addition, we also mentioned the corresponding pressures in the text.

(b) “The cyan box in TRACZILLA show likely convective influences while ATLAS shows none. Why the two models are showing such different results?”

After the review, we noticed that there was a missing line in the analysis code. The enhancement in the TRACZILLA cyan box was corresponding to trajectories that were leaving the meteorological domain at higher altitudes, and they were not actually associated with convection. After applying the correct analysis, the structures of convective influence are very similar between the two models.

“Also, overall, I can see TRACZILLA shows more convective influences than ATLAS. How can you assess which one is more accurate?”

The differences in the intensity of the convective influences between ATLAS and TRACZILLA are expected and are related to the different approaches used in the two methods, both relying on a different set of assumptions.

In ATLAS, the convective influence is estimated from the modeled detrainment rates of ECMWF ERA5 with a stochastic approach.

In TRACZILLA, the convective influence is estimated from the satellite-observed thick and high clouds. This has the advantage to give an observation-based information on the convective events based on a high temporal and spatial resolution (15 and 20 minutes and 3 and 2 km for MSG1 and Himawari data, respectively), reducing the spatial and temporal uncertainties of their identification with respect to the model-based approach. However, there are uncertainties in the determination of cloud altitudes using only passive sensors, and we have no information on the amount of mixing with ambient air at the point where the backward trajectories hits the cloud.

To conclude, ATLAS and TRACZILLA use different methods relying on different data sets (cloud satellite measurements and ERA5 detrainment rates), which have different temporal and spatial resolutions. It is expected to have different results from these different models. However, it is out of the scope of the paper to compare the two models and, in addition, it would be difficult to assess the performances of the two models from this specific case study. This issue is instead more extensively treated in the following papers: Bucci et al. (2020; 10.5194/acp-2019-1053), Legras and Bucci (2019; 10.5194/acp-2019-1075), and Wohltmann et al. (2019; 10.5194/gmd-12-4387-2019). The intent of this manuscript is to exploit the complementary information from the two models to interpret the data.

We added to the manuscript: *The different absolute percentages for convection probability for ATLAS and TRACZILLA are likely the result of the different underlying data sets and different methods for detection of convection along the backward trajectories by the models.*

P14-P15, the discussion on various air mass signatures. For clarity and easy-to-follow purposes, I highly recommend you assemble all this information into a table. In the table, please list the type of targeting air masses, altitude at which they are sampled, surface regions where they were originated from, average measured HNO₃, O₃, PAN, C₂H₂, HCOOH concentrations within these colored boxed, transport time since they left the surface, etc. Second, please add a summary discussion on the different chemical signature of airmasses from different regions, e.g. the purple/blue box air from the marine background vs. the orange/red box air from China, etc.

(1) We followed the suggestion of the referee and added such a table to the manuscript.

(2) We expanded the discussion at the end of Sec. 4.

Sections 5 & 6. I found the observation-model comparison and evaluation a major weakness of this study. Neither CAMS nor EMAC produces well the observed features and gradients of all five species. This is particularly the problem for C₂H₂ and HCOOH. I also have problems with the brutal way of increasing NMVOC emissions by 50% and 100%. I don't see any improvements in model performance with such approach. By matching with observations better in a few patchy spots, you are also creating huge biases in other places (Figure 6) for all three species. PAN, C₂H₂ and HCOOH can be emitted and/or formed from various sources, i.e. anthropogenic emissions and biomass burning emissions being the highly relevant sources. The differences in the regional distributions of these sources can have a dominant impact on tropospheric distribution of these gases after they are being lofted and formed during transport. A proper way to address this model bias is to adjust the emission strength of these individual sources in separate runs and assess how do the resulted distribution change. This way, one can potentially assess the sources of these biases. You are only presenting analysis of one single flight. Therefore, such model sensitivity simulations can be easily conducted within a few days. The new model results and the corresponding discussion should be included in the revised manuscript before the paper is moving forward for publication.

We agree that the sensitivity test performed with EMAC is a very simple analysis, based on the findings by Monks et al. (2018), and not a full sensitivity study. Unfortunately, we do not share the referee's optimism to perform a full sensitivity study "easily [...] within a few days", given our workforce and computational resources. Even though we only compare and discuss one flight, every sensitivity simulation needs to include the time of at least several weeks before the measurement, in order to account for the transport of pollution from the boundary layer to the upper troposphere, where the measurements are performed.

For that reason, we decided to remove Sec. 6 from our manuscript, show results of the simple sensitivity test with +50% increased NMVOC emissions in the supplementary materials, and only briefly summarize the results of this test in Sec. 5. We think that the comparisons of GLORIA measurements to

CAMS and EMAC without a detailed sensitivity study are of value on their own, as these comparisons point out considerable weaknesses of well-known atmospheric models in the upper troposphere of the ASM. In our opinion, it is also important to document negative outcomes of model evaluation studies, in order to motivate further sensitivity studies and model improvements.

Pollution trace gas distributions and their transport in the Asian monsoon upper troposphere and lowermost stratosphere during the StratoClim campaign 2017

Sören Johansson¹, Michael Höpfner¹, Oliver Kirner², Ingo Wohltmann³, Silvia Bucci⁴, Bernard Legras⁴, Felix Friedl-Vallon¹, Norbert Glatthor¹, Erik Kretschmer¹, Jörn Ungermann⁵, and Gerald Wetzel¹

¹Institute of Meteorology and Climate Research, Karlsruhe Institute of Technology, Karlsruhe, Germany

²Steinbuch Centre for Computing, Karlsruhe Institute of Technology, Karlsruhe, Germany

³Alfred Wegener Institute, Helmholtz Center for Polar and Marine Research, Potsdam, Germany

⁴Laboratoire de Méétéorologie Dynamique, UMR8539, IPSL, CNRS/PSL-ENS/Sorbonne Université/École polytechnique, Paris, France

⁵Institute of Energy and Climate Research - Stratosphere (IEK-7), Forschungszentrum Jülich, Jülich, Germany

Correspondence: S. Johansson (soeren.johansson@kit.edu)

Abstract. We present the first high resolution measurements of pollutant trace gases in the Asian Summer Monsoon Upper Troposphere and Lowermost Stratosphere (UTLS) from the Gimballed Limb Observer for Radiance Imaging of the Atmosphere (GLORIA) during the StratoClim (Stratospheric and upper tropospheric processes for better climate predictions) campaign ~~with base~~ based in Kathamandu, Nepal, 2017. Measurements of peroxyacetyl nitrate (PAN), acetylene (C₂H₂), and formic acid (HCOOH) show strong local enhancements up to altitudes of 16 km. More than 500 pptv of PAN, more than 200 pptv of C₂H₂, and more than 200 pptv of HCOOH are observed. ~~An observed local maximum~~ Air masses with increased volume mixing ratios of PAN and C₂H₂ at altitudes up to 18 km, reaching to the lowermost stratosphere, ~~instead has been transported for a longer time~~ were present at these altitudes for more than 10 days, as indicated by trajectory analysis. A local minimum of HCOOH is correlated with a previously reported maximum of ammonia (NH₃), which suggests different wash out efficiencies of these species in the same air masses. ~~To study the influence of convective transport to the measured pollution trace gas occurrences in detail, a trajectory analysis of~~ A backward trajectory analysis based on the models ATLAS and TRACZILLA ~~examined backward trajectories, using advanced techniques for detection of convective events, and~~ starting at geolocations of GLORIA measurements with enhanced pollution trace ~~gases. Both trajectory schemes implemented advanced techniques for detection of convective events. These convective events~~ gas concentrations has been performed. The analysis shows that convective events along trajectories leading to GLORIA measurements with enhanced pollutants are located close to regions, where satellite measurements by ~~OMI show the~~ Ozone Monitoring Instrument (OMI) indicate enhanced tropospheric columns of nitrogen dioxide (NO₂) in the days prior to the observation. ~~As an application of these highly resolved measurements, a~~ A comparison to the ~~atmospheric models CAMS and EMAC is~~ global atmospheric models Copernicus Atmosphere Monitoring Service (CAMS) and ECHAM/MESSy Atmospheric Chemistry (EMAC) has been performed. It is ~~demonstrated that these~~ simulation results shown that these models are able to reproduce large scale structures of the pollution trace gas distributions ~~if the convective influence on the measured air masses is captured by the meteorological fields used by these simulations.~~

~~Both models do not have sufficient horizontal resolution to capture all the for one part of the flight, while the other part of the flight reveals large discrepancies between models and measurement. These discrepancies possibly result from convective events that are necessary to reproduce the fine structures measured by GLORIA. To investigate the influence of the strength of non-methane volatile organic compounds (NMVOCs) emissions in the EMAC model, sensitivity studies with artificially enhanced NMVOC emissions are performed. With these enhanced emissions, the simulation results succeed to reproduce the measured peak values of the pollutants, but do not improve the comparison of spatial distributions not resolved or parameterized in the models, uncertainties in the emissions of source gases, and uncertainties in the rate constants of chemical reactions.~~

1 Introduction

During the Asian Summer Monsoon (ASM), a large-scale persistent anticyclonic circulation, the so-called Asian Monsoon Anticyclone (AMA), exists in the upper troposphere. Convective processes are able to inject polluted lower tropospheric air masses into the AMA (Randel and Jensen, 2013; Vogel et al., 2015; Pan et al., 2016; ?; Legras and Bueci, 2019) (Randel and Jensen, 2013; Vogel et al., 2015; Pan et al., 2016; Legras and Bueci, 2019). So far, most observational information of the Upper Troposphere and Lowermost Stratosphere (UTLS) composition during the ASM has been obtained by satellite limb-sounding experiments (e.g., Santee et al., 2017) which are, however, restricted by low relatively coarse vertical and horizontal resolution and sampling. Airborne in-situ observations of air masses inside air masses belonging to the AMA are extremely sparse and often sample only filaments or the border areas, border areas, or outflow of the AMA. Here (e.g., Bourtsoukidis et al., 2017; Gottschaldt et al., 2018). Here, we present data from the first dedicated aircraft campaign sampling air from the central region of the AMA.

In the contemporary understanding, the chemical composition of the confined system of the AMA is dominated by enhanced amounts of tropospheric trace gases, such as water vapor (H_2O) and carbon monoxide (CO), which are transported to higher altitudes (Santee et al., 2017). Several model studies have identified the impact of different source regions and long-range transport on the AMA, either with artificial tracers (e.g., Vogel et al., 2015, 2016, 2019) or e.g., CO as a proxy (Pan et al., 2016; Cussac et al., 2020). However, large discrepancies are observed in ASM radiative heating rates between different reanalyses (Randel and Jensen, 2013), which result in uncertainties in diabatic vertical transport. Together with large uncertainties in vertical transport due to convection (e.g., Hoyle et al., 2011), atmospheric models are limited in their ability to simulate air masses within the ASM. Comparisons of pollutant trace gas observations in the upper troposphere with simulation results may help to identify problems in atmospheric models.

It has been shown that pollutants, such as ammonia (NH_3) or peroxyacetyl nitrate (PAN) are first transported to the upper troposphere and then confined there until the breakup in late summer accumulated there (Höpfner et al., 2016; Ungermann et al., 2016). These pollutants play an important role in the formation of upper tropospheric ozone and aerosol (Singh, 1987; Höpfner et al., 2019) (e.g., Singh, 1987; Höpfner et al., 2019). Airborne in-situ measurements of filaments with polluted monsoon air masses during the ESMVal (Earth System Model Validation) campaign have revealed that O_3 increases in the AMA outflow in tropospheric air (Gottschaldt et al., 2018). Based on in-situ measurements of another aircraft campaign (Oxidation Mechanism Observations), Lelieveld et al. (2018) formulated the picture of the AMA as a pollution pump and purifier by OH hydroxyl radicals (OH)

of the polluted air masses, originating from South Asian emissions: Due to the production of OH by reactions with lightning nitrogen oxide (NO_x) in the upper troposphere, the polluted air masses are processed with the available OH. ~~Several model studies identified the impact of different source regions and long-range transport to the AMA, either with artificial tracers (e.g., Vogel et al., 2015, 2016, 2019) or e.g., CO as a proxy (Pan et al., 2016; Cussac et al., 2020). Large discrepancies~~
5 ~~are observed in radiative heating rates and upward transport between different reanalyses (Randel and Jensen, 2013). However, observational data of the chemical composition of the upper troposphere inside the ASM~~ Besides these measurements of filaments and outflow air, observations of the ASM UTLS in high spatial resolution are sparse.

The first ~~observations of the upper tropospheric chemical composition in high vertical resolution aircraft observations sampling air in the center of the AMA~~ have been obtained during the high-altitude airborne StratoClim (Stratospheric and
10 upper tropospheric processes for better climate predictions) campaign. This study presents ~~and discusses~~ a unique data set of pollution trace gases ~~measured during this campaign~~, in particular non-methane volatile organic compounds (NMVOCs) ~~, in the Asian monsoon UTLS. StratoClim has been the first high-altitude airborne campaign with observations in the UTLS inside the AMA. These data were~~ obtained with the Gimbalbed Limb Observer for Radiance Imaging of the Atmosphere (GLORIA)
15 during this StratoClim ~~aircraft campaign 2017, with base~~ campaign based in Kathmandu, Nepal ~~, 2017~~. One goal of the GLO-RIA measurements was to identify and quantify the spatial distribution of the pollution trace gases PAN, C₂H₂, and HCOOH, together with HNO₃ and O₃ in the Asian monsoon UTLS. ~~In addition, atmospheric chemistry models that simulate the Asian monsoon are sparsely evaluated due to the low number of detailed observations in the UTLS.~~

In this study, we ~~apply this unique set of NMVOC measurements in the UTLS during the Asian monsoon in two directions~~ use the NMVOC measurements from GLORIA collected during StratoClim to address two important science objectives. First,
20 the origin of polluted air masses is investigated through two trajectory models allowing advanced schemes for detection of convective vertical transport times and areas. Second, a first evaluation ~~of two~~ in the ASM UTLS in high spatial resolution of the atmospheric chemistry models ~~is provided and suggests improvements for these models based on the comparisons with the GLORIA measurements~~ EMAC and CAMS is provided.

In the following section, methods and data sets are introduced: ~~The~~ First, the discussed pollution trace gases are briefly
25 characterized, the StratoClim aircraft campaign is described and the GLORIA measurements and data evaluation explained, and the atmospheric models applied here are introduced. Then, the GLORIA measurements are discussed (~~section~~ Section 3); ~~followed by~~. This is followed by a presentation of the analysis of ATLAS and TRACZILLA backward trajectories from regions air masses of interest identified by the GLORIA measurements (~~section~~ Section 4). ~~The following section (section 5)~~ Section 5 presents a comparison to the atmospheric chemistry models EMAC and CAMS. ~~The last section before the conclusion~~
30 ~~(section ??) discusses the influence of increased NMVOC emissions in the EMAC model.~~

2 Data sets and methods

2.1 Measured trace gases

The scientific analysis of the trace gas measurements will be based on ~~five species,~~ the five species HNO₃, O₃, PAN, C₂H₂, and HCOOH, which are briefly introduced in the following paragraphs. Focus is put on sources and sinks of these species, their lifetimes in the atmosphere, and reports of earlier measurements.

2.1.1 Nitric acid

Nitric acid (HNO₃) is a trace gas with maximum mixing ratios of several ppbv in the stratosphere (e.g., Brasseur and Solomon, 2005). In the troposphere, HNO₃ typically has mixing ratios of less than 1 ppbv. Atmospheric HNO₃ acts as a sink of tropospheric ~~nitrogen-oxide (NO_x ; (e.g. :-, NO₂+OH→ HNO₃))~~ but is also part of a variety of other chemical reactions, which are not mentioned here in detail (see e.g., Burkholder et al., 2015). Tropospheric NO_x may result from fossil fuel combustion, biomass burning, lightning, soil emissions, and stratospheric intrusions (Schumann and Huntrieser, 2007).

There is a large number of spaceborne HNO₃ observations reaching down into the upper troposphere, e.g., volume mixing ratio (VMR) profiles from the Microwave Limb Sounder (~~MLS; ?Santee et al., 2007~~)(MLS; Santee et al., 2007, 2011), the Atmospheric Chemistry Experiments - Fourier Transform Spectrometer (ACE-FTS; Wolff et al., 2008), or the Michelson Interferometer for Passive Atmospheric Sounding on the Envisat satellite (~~von Clarmann et al., 2009, MIPAS~~)(MIPAS; von Clarmann et al., 2009). Airborne measurements have been performed in-situ using chemical ionization mass spectrometer techniques (e.g., Neuman et al., 2001; Jurkat et al., 2016), and also with remote sensing techniques (e.g., Braun et al., 2019). In the ASM, HNO₃ is used as a stratospheric tracer to demonstrate the isolation of the AMA (Park et al., 2008) and ~~within the~~ is used for studies of transport and chemistry of ~~PAN (Fadnavis et al., 2014)~~peroxyacetyl nitrate (PAN; Fadnavis et al., 2014). In this paper, HNO₃ measurements serve as complementary information and are not analyzed in detail.

2.1.2 Ozone

Ozone (O₃), ~~similar~~ similarly to HNO₃, has its maximum in the stratosphere, but with much higher mixing ratios of several ppmv (e.g., Brasseur and Solomon, 2005). Due to the importance of the stratospheric ozone layer, stratospheric O₃ is continuously monitored (WMO, 2019). ~~Tropospheric enhancements of~~ In the ASM troposphere, O₃ typically can reach up to several hundred ppbv ~~has typical background values of 25-150 ppbv (e.g., Brunamonti et al., 2018)~~. Sources of tropospheric O₃ are stratosphere-troposphere exchange processes, and ~~catalytic reactions with nitrogen oxides (Brasseur and Solomon, 2005)~~ in situ production from NO_x and hydrogen oxide radicals, and from NO_x and peroxide radicals from oxidation of volatile organic compounds (Brasseur and Solomon, 2005; Bozem et al., 2017). Thus, tropospheric O₃ can be an indicator of polluted air masses. Furthermore, lightning NO_x may increase tropospheric ozone. Tropospheric enhancements of O₃ typically can reach up to several hundred ppbv. Loss of tropospheric O₃ is caused by photolysis, ~~and~~ reactions with OH, and reactions with NO_x (e.g., Bozem et al., 2017). For that reason, moist and clean air masses are correlated with rather low O₃ mixing ratios.

During the Asian monsoon, typically low tropospheric O₃ mixing ratios are measured due to uplift of moist and clean air from the Indian ~~ocean~~ (Safieddine et al., 2016) ~~Ocean~~ (e.g., Safieddine et al., 2016; Santee et al., 2017; Brunamonti et al., 2018).

Measurements of O₃ in the upper troposphere are available e.g., VMR profiles from MLS (Froidevaux et al., 1994; Livesey et al., 2008), ACE-FTS (Sheese et al., 2016), MIPAS (von Clarmann et al., 2009), from airborne in-situ (e.g., Browell et al., 1987; Zahn et al., 2012; Safieddine et al., 2016) and airborne remote sensing measurements (e.g., Browell et al., 1987; Woiwode et al., 2012). During recent Asian monsoon seasons, balloon-borne ozone sondes have been launched (e.g., Bian et al., 2012; Brunamonti et al., 2018; Li et al., 2018). Similarly to HNO₃, ~~measurements of enhanced O₃ in the ASM is used as an~~, ~~within the generally O₃-poor AMA upper tropospheric air, is either interpreted as indicator of stratospheric air masses and of polluted air~~ (Park et al., 2007, 2008) (e.g., Park et al., 2007, 2008) or connected to uplift of O₃ precursor species of polluted air (Gottschaldt et al., 2017).

2.1.3 Peroxyacetyl nitrate

~~Peroxyacetyl nitrate (PAN)~~ PAN is a secondary pollutant formed by the reaction of peroxyacetyl with nitrogen dioxide:



Peroxyacetyl is a product of oxidation or photolysis of NMVOC, which are emitted from fuel combustion and biomass burning (Fischer et al., 2014). PAN is mainly destroyed by thermal decomposition to the starting species of reaction (R1), whereas dry deposition and photolysis play a minor role ~~at lower tropospheric altitudes~~ (e.g., Fadnavis et al., 2014). ~~In the upper troposphere instead, photolysis is the dominant loss process for PAN~~ (e.g., Fadnavis et al., 2015). While the lifetime of PAN is very short at lower altitudes ~~due to rapid thermal decomposition~~ (1 h at ~~temperatures of~~ 298 K), it becomes progressively longer and reaches around 5 months at higher altitudes (~~at temperatures of~~ 250 K). ~~Typical background abundances of PAN in the upper troposphere are below 100 pptv~~ (Glatthor et al., 2007). This makes PAN useful as a tracer for upper tropospheric transport studies (Singh, 1987; Glatthor et al., 2007; Fischer et al., 2014).

PAN VMR observations are reported from the spaceborne instruments ACE-FTS (Coheur et al., 2007), MIPAS-Envisat (Glatthor et al., 2007; Wiegeler et al., 2012), CRISTA (~~Ungermann et al., 2016~~) (~~Cryogenic Infrared Spectrometer and Telescope for the Atmosphere~~), and column information from IASI (Infrared Atmospheric Sounding Interferometer; Coheur et al., 2009). Airborne measurements were achieved from instruments with remote sensing (CRISTA-NF; Ungermann et al., 2013), and in-situ (e.g., Singh et al., 2001) measurement techniques. In the ASM, measurements of PAN have been applied to study transport and impact of polluted air masses (Fadnavis et al., 2014). Typically, PAN is strongly enhanced within the main part of the AMA (Ungermann et al., 2016).

2.1.4 Acetylene

Acetylene or ethyne (C₂H₂) ~~is a tropospheric substance with mixing ratios of few pptv in maximum and a product of combustion of bio- and fossil fuels~~, ~~a product of biofuel and fossil fuel combustion~~ and biomass burning, ~~has maximum tropospheric mixing ratios of a few ppbv~~. Typical background values for C₂H₂ in the tropics are below 75 pptv (e.g., Xiao et al., 2007; Wiegeler et al., 2011).

The reaction with OH is the major sink of C₂H₂ in the troposphere. Compared to PAN, C₂H₂ has a rather short lifetime of 2 weeks (Xiao et al., 2007). Measurements of C₂H₂ VMR profiles have been reported by e.g., ATMOS (Rinsland et al., 1987) (Atmospheric Trace Molecule Spectroscopy; Rinsland et al., 1987), ACE-FTS (Rinsland et al., 2005), and MIPAS-Envisat (Wiegele et al., 2012). Within the ASM, measurements of C₂H₂ have been used as tropospheric tracer to study the chemical isolation of the AMA (Park et al., 2008).

2.1.5 Formic acid

Formic acid (HCOOH) mainly exists in the troposphere (with ~~mixing ratios~~ background VMRs below 100 pptv and peak VMRs smaller than 1 ppbv (Grutter et al., 2010)) and originates from biogenic emissions, biomass burning, and fossil fuel combustion (Mungall et al., 2018). In contrast to PAN and C₂H₂, HCOOH is water soluble, such that its major tropospheric sink is wet deposition (depending on acidity). Further sinks are reaction with OH, and dry deposition (Paulot et al., 2011). The average atmospheric lifetime is estimated to be 2-4 days, while the lifetime is shorter in the boundary layer and longer in the free troposphere (Millet et al., 2015). Measurements of atmospheric HCOOH VMR profiles are available e.g., from ACE-FTS (Rinsland et al., 2006), MIPAS-Envisat (Grutter et al., 2010) and column information from IASI (Coheur et al., 2009). Airborne measurements in the UTLS are reported by e.g., Reiner et al. (1999) ~~or~~ and Singh et al. (2000). To our knowledge, no studies using measurements of HCOOH in the ASM upper troposphere have been published so far.

2.2 StratoClim aircraft campaign and GLORIA observations

During the Asian summer monsoon 2017, the StratoClim aircraft campaign was ~~performed with basis in~~ conducted from Kathmandu, Nepal. In total, 22 in-situ and 3 remote sensing instruments were integrated into the Russian high altitude ~~high altitude~~ research aircraft M55 Geophysica. As part of the remote sensing payload, GLORIA was deployed during four research flights of this measurement campaign. In ~~this the present~~ work, we will discuss the research flight on 31 July 2017. ~~The flight path of this deployment~~ This research flight was selected for this work due to high flight altitudes and low cloud top altitudes within the AMA, which both are optimal measurement conditions for the infrared limb sounding instrument GLORIA. This research flight was by far the best due to the flight length allowing different air masses to be sampled, and due to the low cloud top altitude. The related flight path is shown in Fig. 1.

GLORIA is a unique airborne imaging limb infrared sounding instrument (Friedl-Vallon et al., 2014; Riese et al., 2014), which has been operated during several campaigns with the German HALO research aircraft and with M55 Geophysica. The main part of GLORIA is a Michelson Fourier Transform Spectrometer combined with an imaging detector, which allows for simultaneous measurements of 127 × 48 spectra. Further, GLORIA consists of two external black bodies for in-flight radiometric calibration and a gimbal frame for active corrections of aircraft movements and ~~line-of-sight~~ line-of-sight control. Interferograms used in this study are from the “high spectral resolution” mode with 8.0 cm optical path difference, which results in spectra with 0.0625 cm⁻¹ sampling.

These measured spectra are then used to retrieve profiles of atmospheric trace gases and particles. The retrieval is performed using a nonlinear least-squares fit with Tikhonov regularization. The overall retrieval strategy is explained in detail by Johans-

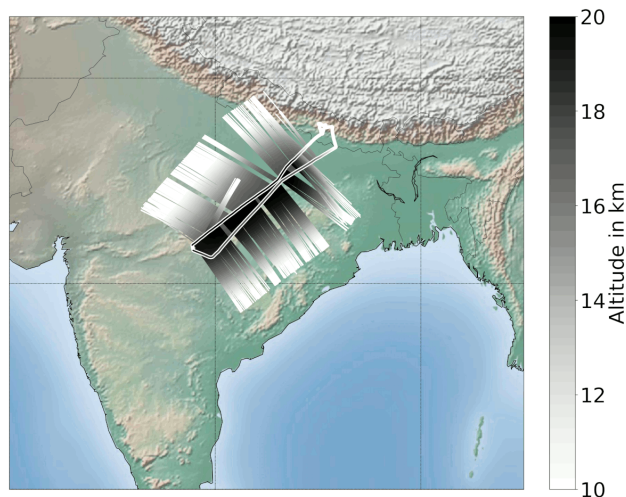


Figure 1. Flight path and tangent altitudes of StratoClim research flight on 31 July 2017. The bold line indicates the flight path and aircraft altitude of Geophysica, while small across-track lines indicate the ~~position-positions~~ and ~~altitude-altitudes~~ of tangent altitudes of GLORIA measurements. The map is centered at the Indian subcontinent.

son et al. (2018). ~~Main differences compared to this retrieval strategy are~~ The retrieval strategy used here differs from that described by Johansson et al. (2018) mainly in the applied cloud filter and the handling of continua in the radiative transfer model KOPRA (Stiller, 2000): Due to the high mixing ratios of aerosols (Höpfner et al., 2019), cloud filtering using the MIPAS "cloud index" method (Spang et al., 2004) was replaced by filtering according to mean radiance between 850 cm^{-1} and 970 cm^{-1} with a threshold of $800\text{ nW (cm}^2\text{ sr cm}^{-1})^{-1}$. Due to highly structured distributions of aerosol and thin cirrus, the retrieval of a spectrally flat extinction was ~~substituted by retrieving~~ replaced by retrieval of a multiplicative scale and an additive radiance offset parameter for each vertical point in the retrieval altitude grid. For the HNO_3 retrieval, a pre-fitted scale from the spectral region $955.8750 - 958.4375\text{ cm}^{-1}$ has been used and only the offset was fitted (instead of scale and offset). Spectral ranges for the retrievals for each discussed trace gas and the handling of interfering species are summarized in Tab. 1, together with typical vertical resolutions and estimated errors. Detailed plots of estimated errors and vertical resolutions are provided as supplement ~~of to~~ this paper.

2.3 Atmospheric model simulations

2.3.1 EMAC

The ECHAM/MESSy Atmospheric Chemistry (EMAC) model is a numerical chemistry and climate simulation system that includes sub-models describing tropospheric and middle ~~atmosphere-atmospheric~~ processes and their ~~interaction-interactions~~ with oceans, land, and human influences (Jöckel et al., 2010). It uses the second version of the Modular Earth Submodel System (~~MESSy2MESSy~~) to link multi-institutional computer codes. The core atmospheric model is the 5th generation European Cen-

Table 1. Retrieval properties for HNO₃, O₃, PAN, C₂H₂, and HCOOH: ~~Used-spectral~~Spectral regions ~~used~~, and handling of interfering species. 10 and 90 percentile ranges are given for vertical resolution and estimated errors. In the supplement, it is shown that larger absolute errors are typically connected to higher VMRs.

Target <u>target</u> gas	spectral regions in cm ⁻¹	fitted species	forward-calculated species	vertical resolution	estimated error
HNO ₃	867.0000 - 870.0000	HNO ₃ , NH ₃ , OCS	H ₂ O [†]	0.7 - 0.9 km	70 - 220 pptv
O ₃	780.6250 - 781.7500 985.0000 - 988.0000	O ₃	H ₂ O, CO ₂	0.5 - 1.3 km	70 - 200 ppbv
PAN	780.3125 - 790.0000 794.0000 - 805.0000	PAN, H ₂ O, O ₃ , CCl ₄	CO ₂ , HNO ₃ [†] , CFC-22, CFC-113, ClONO ₂ , HNO ₄	0.5 - 0.8 km	50 - 120 pptv
C ₂ H ₂	759.5625 - 759.8125 766.5625 - 766.8125 775.9375 - 776.3125 780.5000 - 780.8750	C ₂ H ₂ , O ₃	H ₂ O [†] , CO ₂ , NO ₂ , NH ₃ [†] , HNO ₃ [†] , HCN, CH ₃ Cl, C ₂ H ₆ [†] , COF ₂ , CFC-22, CCl ₄ , N ₂ O ₅ , ClONO ₂ , CH ₃ CCl ₃ , PAN [†]	0.7 - 1.0 km	30 - 60 pptv
HCOOH	1103.5000 - 1106.1250 1112.5000 - 1116.8750	HCOOH	H ₂ O [†] , O ₃ [†] , CH ₄ CFC-11, CFC-12, CFC-113	0.7 - 1.0 km	30 - 70 pptv

[†] Results of previous retrievals (not necessarily shown in this paper) targeting these species have been used for simulation of the spectra.

tre Hamburg general circulation model (~~ECHAM5, version 5.3.02~~Roeckner et al., 2006)(ECHAM5; Roeckner et al., 2006). For the present study, we applied EMAC (ECHAM5 version 5.3.02, MESSy version 2.53) in the ~~T106L90MA-resolution~~T106L90MA resolution, i.e. with a spherical truncation of T106 (corresponding to a quadratic Gaussian grid of approx. 1.125~~by~~^o × 1.125~~degrees in latitude and~~^o (latitude × longitude) with 90 vertical hybrid pressure levels ~~of~~ up to 0.01 hPa (approx. 80 km). ~~The chemistry setup in~~For convection, we use the parameterization introduced by Tiedtke (1989) with modifications by Nordeng (1994) as described in Tost et al. (2006). The chemical setup of the chemistry submodel MECCA (?)-was expanded (in contrast to the standard chemistry) with regard to a better (Sander et al., 2011) was selected with focus on the simulation of PAN and ~~the~~ tropospheric chemistry. It comprises 460 chemical substances, 1187 gas phase reactions, and 262 ~~photolyses-~~ photolysis reactions. The boundary conditions in our simulation are similar as in the EMAC hindcast simulations within the ESCiMo project (Earth System Chemistry integrated Modelling; Jöckel et al., 2016) and CCMI project (Chemistry-Climate Model Initiative), which among others were performed for the WMO report “Scientific Assessment of ozone depletion” (WMO, 2019). The boundary conditions for the mixing ratios of the greenhouse gases are from the RCP 6.0 scenario (Representative Concentration Pathway; MIP6). For the emission of NMVOCs, a data set of the MACCity emission inventory (MACC/CityZEN; Granier et al., 2011) and a data set consisting of a combination of ACCMIP (Atmospheric Chemistry and Climate Model Intercomparison Project; Lamarque et al., 2013) and RCP 6.0 data (Fujino et al., 2006) were considered. There are anthropogenic emissions sources from biomass burning, agricultural waste burning, fossil fuels, ship, road and aircraft emissions, as well as biogenic emissions. For the simulated year 2017, the emissions of the year 2010 (the most recent year available) are repeated. We performed a standard simulation

and ~~two sensitivity simulations~~ a sensitivity simulation with additional 50% ~~and additional 100%~~ emissions of NMVOC. ~~In all three simulations~~ Thereby, the emissions were increased globally in all NMVOC emission sources by 50%. In both simulations, the meteorological fields were specified by ~~ECMWF ERA-Interim (Dee et al., 2011)~~ the European Centre for Medium-Range Weather Forecasts (ECMWF) European Reanalysis Interim (ERA-Interim; Dee et al., 2011), and all simulations were initial-
5 ized on 1 May 2017.

2.3.2 CAMS

The Copernicus Atmosphere Monitoring Service (CAMS) reanalysis (CAMSRA) ~~from the European Centre for Medium-Range Weather Forecasts (ECMWF) of ECMWF~~ is an atmospheric composition model, focusing on the troposphere. CAMS applies the ECMWF IFS (Integrated Forecast System) model and assimilates various satellite measurements of atmospheric com-
10 position. It uses the chemistry module IFS(CB05) (Flemming et al., 2015) and the aerosol module as ~~described~~ described in Morcrette et al. (2009). Apart from assimilated ozone, CAMS does not simulate stratospheric chemistry. The model uses 60 vertical hybrid pressure levels, with the top level at 0.1 hPa and has a horizontal resolution of 80 km. Output is provided every 3 hours. The data set is characterized in detail by Inness et al. (2019). Anthropogenic emissions are prescribed by MACCity (Granier et al., 2011), biogenic emissions by MEGAN2.1 (Model of Emissions of Gases and Aerosols from Nature; Guenther et al., 2012)
15 , and biomass burning emissions by GFAS v1.2 (Global Fire Assimilation System; Kaiser et al., 2012). CAMS reanalysis data is available for the time between 2003 and 2018. In a model evaluation study by ~~Wang et al. (2020)~~, trace gas measurements from aircraft campaigns were compared to CAMS reanalysis data. Tropospheric profiles (up to 12 km) of O₃, HNO₃, and PAN above Hawaii showed an agreement within the uncertainties of measurement and model. These agreements encourage model evaluation at altitudes of the upper troposphere in the ASM, as presented in this study.

20 2.3.3 TRACZILLA

The TRACZILLA model (Pisso and Legras, 2008) is a modified version of the Lagrangian model FLEXPART (Stohl et al., 2005; Legras et al., 2005). Trajectories are launched at GLORIA tangent points at ~~the a~~ rate of 1000 per point. They are integrated backward in time for one month, using the ECMWF reanalysis horizontal winds (~~ERA-5, European Reanalysis 5, ERA5~~, 1 h temporal resolution), and diabatic vertical motions. The TRACZILLA simulations are run on a $0.25^\circ \times 0.25^\circ$
25 (latitude \times longitude) grid at 137 vertical levels in the spatial domain of 10°W to 160°E , and 0°N to 50°N .

A diffusion with a diffusion coefficient of $D=0.1 \text{ m}^2\text{s}^{-1}$ is added (based on previous studies in the subtropics, Pisso and Legras, 2008; James et al., 2008), represented by a random walk equivalent, that disperses the cloud of parcels from each point. ~~A convective source is then individuated when a trajectory is found~~ trajectory is considered to be influenced by convection if it encounters a convective cloud during its advection with a pressure higher than the ~~pressure of a convective cloud top, as~~
30 ~~similarly done in Tissier and Legras (2016)~~ cloud top pressure (as similarly done by Tissier and Legras, 2016). The location of cloud encounter is then identified as a convective source. We use here the cloud top products provided by the SAF-NWC (EUMETSAT Satellite Application Facility for Nowcasting) software package (Derrien et al., 2010; Sèze et al., 2015) from

MSG1 (Meteosat 8) and Himawari geostationary satellites. More details on the algorithm and its evaluation against trace gas measurements can be found in Bucci et al. (2020) and Legras and Bucci (2019).

2.3.4 ATLAS

Trajectories from the ~~ATLAS~~ Alfred Wegener Institute Lagrangian Chemistry/Transport System (ATLAS) model (Wohltmann and Rex, 2009) are driven by the ~~European Centre for Medium-Range Weather Forecasts European Reanalysis 5 (same ECMWF ERA5)~~ (meteorological fields as TRACZILLA, but with a temporal resolution of 3 h and a horizontal resolution of $1.125^\circ \times 1.125^\circ$ horizontal resolution, 137 vertical levels, 3 h temporal resolution). The model uses a hybrid coordinate transforming from pressure at the surface to potential temperature at the tropopause (Wohltmann and Rex, 2009). In the altitude range of GLORIA, the coordinate is a potential temperature coordinate in good approximation, and the trajectories can be regarded as diabatic trajectories driven by the total heating rates of ERA5. Trajectories are calculated for 30 days prior to the measurement. Time step is 10 minutes.

The trajectory model includes a detailed stochastic parameterization of convective transport driven by ERA5 convective mass fluxes and detrainment rates (Wohltmann et al., 2019). In addition, a vertical diffusion of $D=0.1 \text{ m}^2\text{s}^{-1}$ is added to every trajectory, consistently with TRACZILLA. At every measurement location of GLORIA, 1000 backward ensemble trajectories are started, which take different paths due to the stochastic nature of the convective transport scheme. A convective event is detected by drawing a uniformly distributed random number between 0 and 1 every 10 minutes and comparing that to the calculated probability for detrainment from ERA5 at the location of the trajectory. If the random number is smaller than the calculated probability, it is assumed that a convective event was encountered.

In an analysis of the ATLAS trajectories, the influence of the usage of ERA5 or ERA-Interim as meteorological fields, the influence of applied vertical diffusion, and the influence of the usage of kinematic or diabatic trajectories ~~was investigated (not shown were investigated (shown in Fig. 19 of the Supplementary Information))~~. This analysis (and also similar analyses by Legras and Bucci (2019)) revealed that major differences ~~for the ATLAS trajectories occur between the usage of occur between ATLAS trajectories that use ERA5 or ERA-Interim meteorological fields, while diffusion and kinematic/diabatic trajectories only have minor influences.~~ These major differences are exemplarily visible in Supplementary Fig. 19, where trajectory paths and locations of convective events are considerably different between ERA-Interim and ERA5. Compared to these large discrepancies, differences in trajectory paths and locations of convective events due to the usage of kinematic or diabatic trajectories, or due to the application of vertical diffusion are small.

2.3.5 OMI-NO₂ tropospheric column

2.4 OMI NO₂ tropospheric column

The Ozone Monitoring Instrument (OMI) is a nadir looking ultraviolet-visible spectrometer ~~instrument~~ onboard the NASA Aura satellite. Targeted quantities are columns of trace gases (such as O₃, NO₂, SO₂), aerosol properties, cloud top heights, and surface irradiances (Levelt et al., 2006). In this work, we use the ~~tropospheric~~ tropospheric column of nitrogen dioxide

(NO₂) [version 3](#) as a proxy for pollutant emissions (Crutzen, 1979). OMI [tropospheric column](#) NO₂ is provided as cloud-filtered daily level-3 product on a 0.25° × 0.25° ([latitude × longitude](#)) grid (Krotkov, 2013). [The version 3 standard retrieval of tropospheric column NO₂ comes with a spatial resolution of 1.0° × 1.25° \(latitude × longitude\), and showed an overall agreement with other satellite and ground-based measurements of NO₂ \(Krotkov et al., 2017\).](#) For the analysis in Sec. 4, 14
5 days of OMI NO₂ measurements are averaged to indicate regions of pollutant emissions prior to the measurement.

3 Pollution trace gases measured during StratoClim flight on 2017-07-31

GLORIA measurements of pollution trace gases introduced in Sec. 2.1 are shown as horizontal distributions on a map, and as vertical distributions in Fig. 2, and [regions-air masses](#) that are discussed in this and following sections are marked with colored boxes. As expected, the HNO₃ VMRs (Fig. 2b) strongly increase [a few km](#) above the tropopause ~~at 17, at 19~~ km to
10 typical stratospheric values of more than 2 ppbv. Around the tropopause at 17 km, fluctuations of HNO₃ up to 0.5 ppbv can be observed. In the first part of the flight (until 4:45 UTC), also ~~structures of local enhancements up to 0.5 ppbv are a local maximum of VMRs up to 1.0 ppbv is~~ visible below the tropopause at altitudes between ~~14~~15.5 km and ~~16~~ km. ~~In particular, enhancements are~~ 17 km (close to the red box in Fig. 2b). This maximum is continued by enhancements noted at 16 km at
15 4:00 UTC moving down to 15 km at 4:15-4:50 UTC [with VMRs up to 0.75 ppbv](#) (marked with a magenta box). ~~In the~~ [The shape and position of the red and magenta boxes are optimized for the pollution trace gases PAN and C₂H₂ discussed later in this section to have a local maximum in the red and a local minimum in the magenta box. Thus, these boxes do not exactly match the structure in HNO₃. In addition, Höpfner et al. \(2019\) reported enhanced ammonium nitrate abundances in the red air masses, and a local minimum of ammonium nitrate in the magenta box. Given these different pollution trace gas and aerosol concentrations in the red and magenta boxes, it is assumed that these air masses have different origins, even though the structure in HNO₃ appears to be connected. In the](#) second flight part, at 17 km altitude and 5:45 UTC, a local maximum of 0.5 ppbv
20 HNO₃ is visible, together with a local minimum above, at 18 km altitude.

Measured O₃ (Fig. 2d) shows similar distributions as HNO₃: Above 19 km altitude, elevated VMRs of more than 1000 ppbv are measured in the same region where the HNO₃ measurements show stratospheric values. Above and around the 380 K tropopause, O₃ mixing ratios between 200 ppbv and 400 ppbv are measured. During the second part of the flight, [at](#) around
25 5:30 UTC, a local maximum of O₃ up to 400 ppbv was observed between 15 km and 16.5 km (purple box), but these measurements have relatively high total estimated errors up to ~~180~~160 ppbv, which is within the magnitude of this local enhancement (see Supplementary Fig. 4).

PAN vertical distributions (Fig. 2f) show how different the air masses sampled with GLORIA have been: The first part (until 4:45 UTC) indicates enhanced PAN mixing ratios of more than 500 pptv up to the flight altitude of 18 km. Maximum values
30 are observed at 4:10 UTC at 16 km altitude (marked with a red box). A [PAN](#) local minimum can be found in the same region of the HNO₃ local maximum (magenta box). These retrieved structures come with larger uncertainties compared to other parts of this flight, due to stronger spectral extinction observed at these altitudes in this part of the flight. The rather broadband spectral signature of PAN makes it more difficult for the retrieval to ~~discriminate~~ [distinguish](#) between the spectral offset due to aerosol or

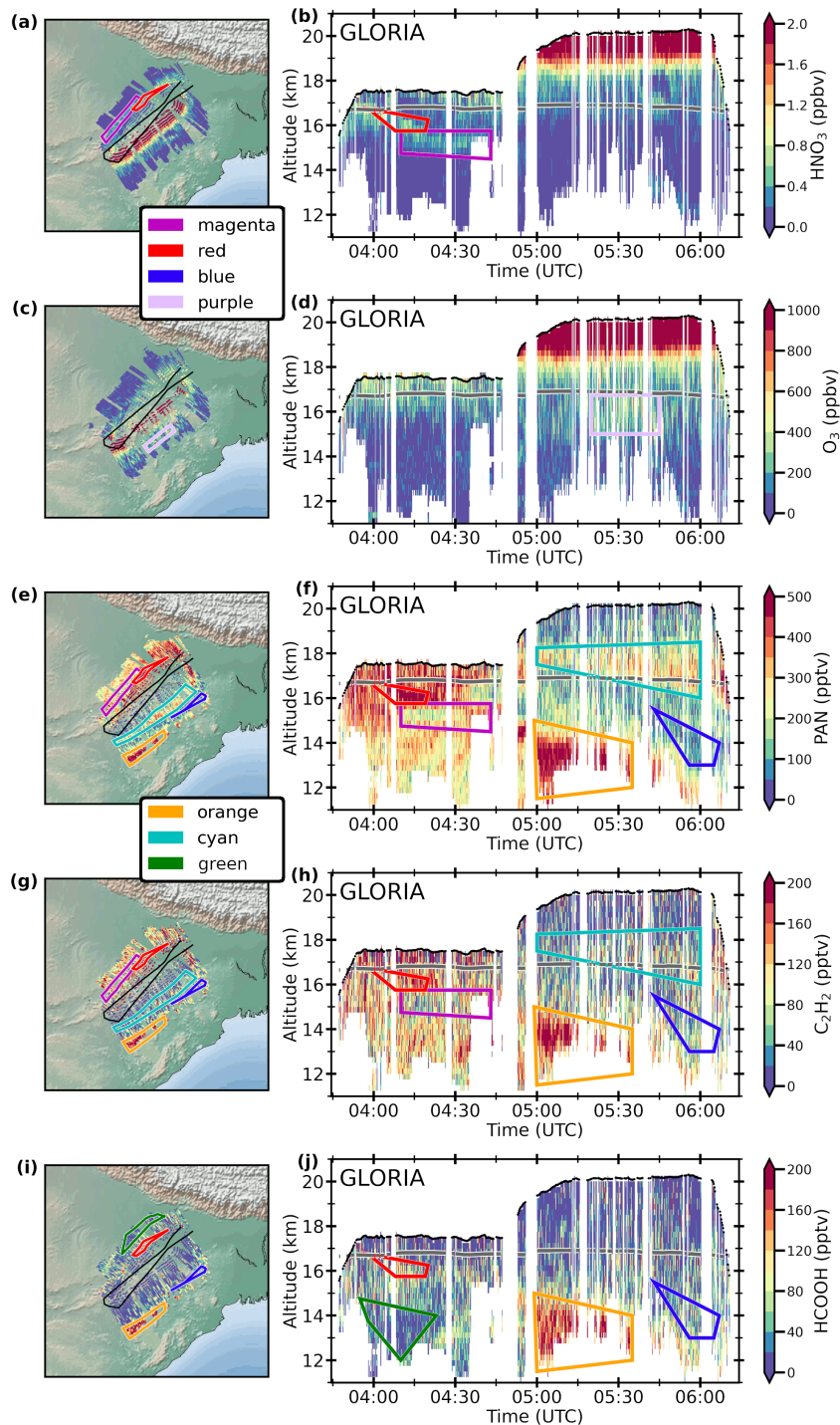


Figure 2. Horizontal (left column) and vertical (right column) distributions of GLORIA measurements of (a-b) HNO₃, (c-d) O₃, (e-f) PAN, (g-h) C₂H₂, (i-j) HCOOH for StratoClim flight on 31 July 2017. The black line in the maps and cross sections shows the flight path, and the green-dark gray line (on the cross section plots only) the 380 K potential temperature isentrope as approximate tropopause altitude. Colored boxes mark regions-air masses of interest, which are discussed in the following sections. The maps are centered at the Indian subcontinent.

5 cirrus clouds, and the targeted spectral emission of PAN. The second part of the flight shows PAN background mixing ratios of 150 pptv in the troposphere and 100 pptv in the stratosphere. At lower altitudes, below 14 km, again enhanced mixing ratios of more than 500 pptv are observed between 5:00 and 5:30 UTC (orange box). Later during this flight, at 6:00 UTC, background values are observed at similar altitudes (blue box). Directly at and above the thermal tropopause, a local enhancement of 250 -

10 ~~As for~~ Similarly to PAN, vertical distributions of C₂H₂ (Fig. 2h) show a large vertical variability during the first part of the flight. A local maximum of up to 200 pptv is observed at 4:10 UTC at 16 km altitude (marked with a red box) and ~~as for PAN~~ a local minimum is visible below (magenta box). Below 14 km altitude, VMRs between 100 pptv and 200 pptv are measured. The second part of the flight shows strong enhancements of C₂H₂ of more than 200 pptv at altitudes below 14 km between

15 5:00 and 5:30 UTC (orange box), where PAN showed enhancements, too. The same local minimum as for PAN is observed at similar altitudes but later during the flight (6:00 UTC, blue box). Above the tropopause (cyan box), ~~a faint~~ there is a minor local maximum with ~~VMRs~~ C₂H₂ VMRs of up to 100 pptv ~~appears in the measurements~~.

Unlike PAN and C₂H₂, HCOOH does not have these enhanced VMRs at and above the tropopause ~~of in~~ the second part of the flight. Enhancements of HCOOH are observed in the first part of the flight at 4:10 and 16 km altitude (red box) and

20 15 at 4:20 and 13 km altitude. In the second part of the flight, as for all ~~other gases~~ gases other than HNO₃ ~~, considerably large~~ and O₃, considerably larger abundances of HCOOH of more than 200 pptv ~~is are~~ observed below 14 km between 5:00 and 5:30 UTC (orange box) and a local minimum is measured at similar altitudes at 6:00 UTC (blue box). ~~In~~ At the beginning of the flight (until 04:15 UTC), below 15 km, a minimum of HCOOH is measured, while PAN and C₂H₂ are present (green box). This is the same region air mass, where Höpfner et al. (2019) reported strongly enhanced mixing ratios of NH₃. This

25 HCOOH local minimum is present, despite enhancements of HCOOH total columns (measured by ~~the Infrared Atmospheric Sounding Interferometer~~; IASI) at the border region between Pakistan and India (see Suppl. Fig. 11), the region identified as source for the enhanced NH₃. The trajectory analysis by Höpfner et al. (2019) indicated transport times of 3 days since convection, which is within the atmospheric lifetime of HCOOH. ~~This~~ The presence of PAN and C₂H₂ ~~and,~~ together with the absence of HCOOH, suggests that the loss of HCOOH was induced by wet deposition, which was more efficient for HCOOH

30 than for NH₃. Both species, HCOOH and NH₃, are water soluble, but HCOOH has a considerably higher Henry ~~coefficient~~ 's Law Constant compared to NH₃. In addition, the solubility is known to be also dependent on the pH of the liquid ~~-(see e.g., Seinfeld and Pandis, 2016)~~ While, HCOOH is acidic, in contrast to NH₃ ~~is alkaline~~, which is alkaline. This difference is a possible explanation for HCOOH being washed out ~~completely~~, while NH₃ is still present in large VMRs in the same air masses. However, we cannot rule out other processes leading to the different behaviors of HCOOH and NH₃ upon transport to

35 the UT, like a difference in retention of these gases upon freezing of the liquid water droplets at high altitudes (Ge et al., 2018). As mentioned above, later during this flight, also strongly enhanced concentrations of HCOOH are observed. This indicates that air masses lifted by convection to high altitudes are not always depleted of HCOOH by washout processes.

The GLORIA measurements show how different the two parts of the flight have been regarding the composition of the measured air masses: In the first part of the flight, high VMRs of all discussed gases tropospheric tracers have been detected

35 up to the tropopause at 17 km, while during the second part of the flight, such high abundances have been only detected at

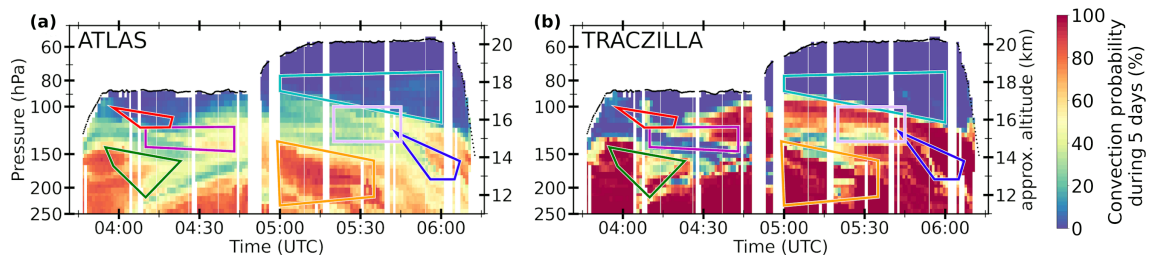


Figure 3. Convection probability of trajectories of the (a) ATLAS and (b) TRACZILLA model starting at the tangent points of the GLORIA measurements. The colors indicate the fraction of trajectories that experienced convection during the five days before the measurement time. Please note that the left vertical axis is shown as pressure in logarithmic scale. For TRACZILLA, pressures below 70 hPa are not shown, as the right vertical axes display an approximation of altitude to facilitate the convection-detection-comparison with cloud-top-temperatures does not work cross section plots in Fig. 2. Colored boxes are repeated from the stratosphere same figure.

altitudes of up to 14 km altitude. This difference between the flight legs is also discussed by Höpfner et al. (2019), who found large abundances of ammonia (NH_3) in the first part of the flight, but none in the second. On the map projections, it can be seen that the tangent points of the measurements point in opposite directions for the different flight parts: Lines of sight of the outbound flight leg point towards north-west and those of the inbound flight leg point towards south-east. In addition, trajectory calculations from-by Höpfner et al. (2019) suggest that air masses observed during the first part of the flight were strongly influenced by convection a few days before the observations. The Below 15 km, the beginning of the second part of the flight shows below 15 km strong enhancements of pollution trace gases, which is and also an indication of convective events (which is discussed later in this paper). The enhancements at and above the tropopause of in the second flight part (cyan box) in PAN and C_2H_2 , but not in HCOOH suggests-, suggest that these air masses are older than a few days (lifetime of HCOOH), but younger than 2 weeks (lifetime of C_2H_2). A detailed analysis of the origin of measured regions air masses of interest (marked by colored boxes) is discussed in Sec. 4.

4 Trajectory analysis: Origin of polluted air masses

To gain more insight about the origin of polluted air through convective processes, here we apply backward trajectories from the models TRACZILLA and ATLAS to estimate-identify the origin of measured polluted air masses. Due to the high-strong influence of convection, which is usually not resolved in the reanalysis data used by the models, both models use advanced methods for the detection of convective events along the trajectories (see Secs. 2.3.3-2.3.4). Fig. 3 shows the fraction of trajectories for each GLORIA measurement time and location that experienced convection during the past 5 days. This fraction is interpreted as convection probability and aides-aids the following interpretation of the origin of polluted air masses. The ATLAS trajectories indicate an enhanced convection probability of more than 50% for the orange and blue marked regions air masses, and parts of the purple and magenta regions-marked air masses also have convection probabilities of 50%, while the red and cyan regions-marked air masses show no noticeable enhancement of convection probability. For the TRACZILLA

trajectories, the convection probabilities are overall higher, but as for ATLAS, the orange and blue region air masses have highest convection probabilities, the purple and magenta region air masses have parts with high convection probability, and the red and cyan regions marked air masses have relatively low convection probabilities. These different absolute percentages for convection probability for ATLAS and TRACZILLA are likely the result of the different methods for detection of convection along the backward trajectories by the models. Another region Another air mass of enhanced convection probability below 15 km (≈ 140 hPa) and earlier than 04:10 UTC is present in both models but not marked by any colored box (green box). This is the part of the flight, where Höpfner et al. (2019) report strongly enhanced ammonia VMRs. In their paper, the same sets of trajectories are used to estimate the source of origin at the border region between Pakistan and India. The different absolute percentages for convection probability for ATLAS and TRACZILLA are likely the result of the different underlying data sets and different methods for detection of convection along the backward trajectories by the models.

In Fig. 4a shows exemplary, we show the origin of the air masses in the colored boxes. As an example, Fig. 4a shows some exemplary 10-day backward trajectories from the ATLAS model released from the orange region of interest (as defined in Fig. 2 and following). Along these trajectories, regions are bordered orange, where the density of convective events along these trajectories is larger than 0.1%, 1.0%, and 10.0%. This density is calculated as started in the orange box (blue lines). In addition, the orange contours in the map show the spatial density of the convective events experienced by the backward trajectories originating in the orange box in the last 10 days. For this, all ensemble trajectories started in the orange box were taken into account (this comprises several GLORIA measurement locations with 1000 ensemble trajectories at each location). Now, the fraction of the number of convective events over the total number of released trajectories from this particular region on a these trajectories that experienced a convective event in a given 1° latitude $\times 1^\circ$ longitude $\times 1^\circ$ longitude grid. I. e. the smallest bordered regions include at least latitude box is calculated for each location on the map. The resulting quantity is a fraction per area, given here in units of percent-per-square-degree. The outermost contours correspond to a density of 0.1 % (or 1.0% and 10.0% for the inner lines) of convective events of all released backward trajectories in a given color, while larger regions contain accordingly a larger fraction. These orange areas are repeated in percent of the started trajectories per square degree. In case that one or two inner contours are present, they correspond to 1 and 10 percent of the started trajectories per square degree, respectively.

To avoid confusion, note that Fig. 3 shows the fraction of the 1000 ensemble trajectories started from each individual GLORIA measurement location that experienced convection in the last 5 days as a function of this measurement location, which is not related to the location of the convective events or grouped by the colored boxes. Fig. 4b, together with the colored areas for the other regions of interest, as defined in shows the same spatial densities as Fig. 2. In the same manner, areas of high density of convective events calculated by TRACZILLA are shown 4a, but now for all colored regions, in boxes and not only for the orange box. Fig. 4c, in shows the same as Fig. 4b, e, in for TRACZILLA. In addition, the OMI NO₂ tropospheric column is shown as an average over 14 days prior to the measurement as a proxy for emission of polluted air masses. These averaged tropospheric NO₂ columns are shown as background in green colors in Fig. 4b and c.

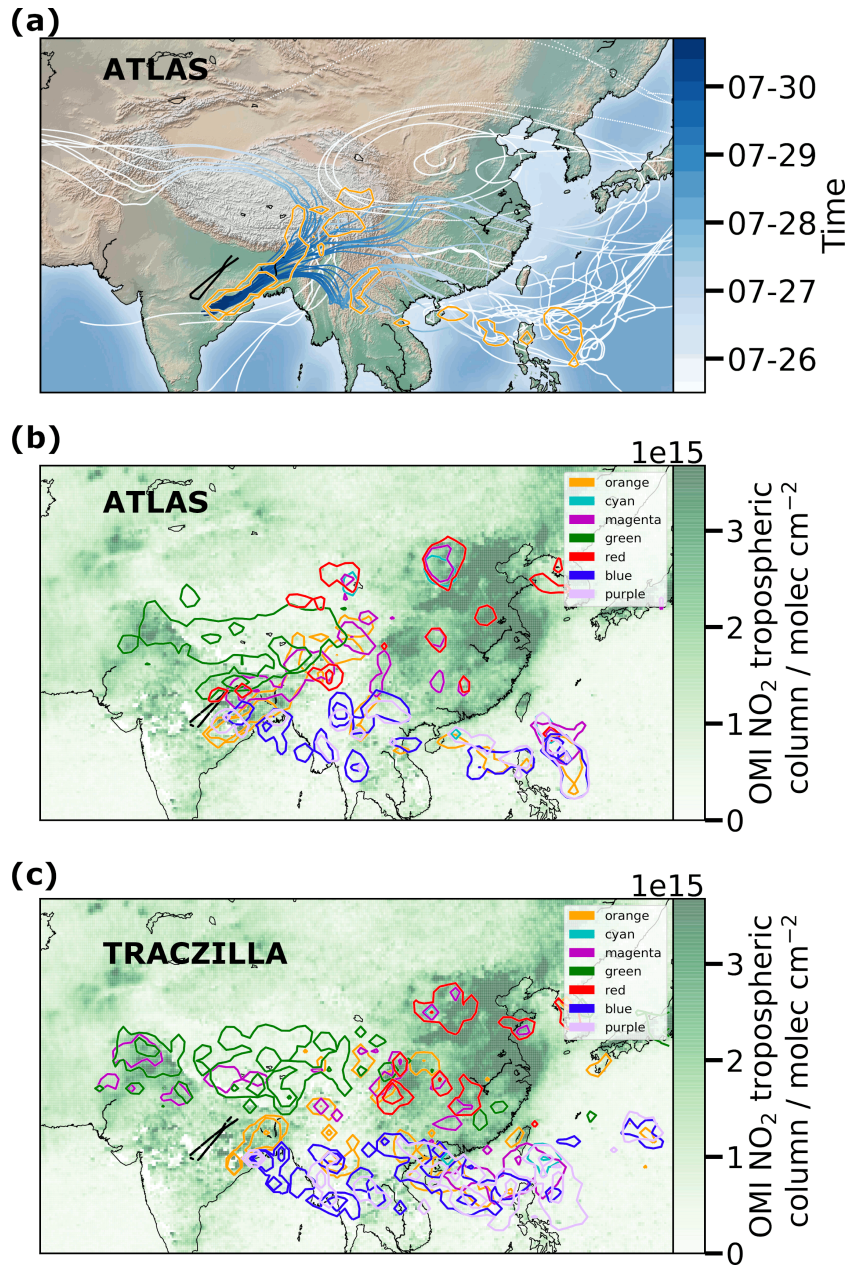


Figure 4. The origin of [regions-air masses](#) of interest along the GLORIA vertical cross sections. (a) Exemplary subset of backward ATLAS trajectories starting at the [region-air masses](#) marked orange in Figs. 2-3. Backward trajectories are displayed in this figure for 10 days, of which the temporal evolution [fo-for](#) the first 5 days [are-is](#) color coded according to the color bar. Orange colored regions on the map mark regions, where the density of convective events (as explained in Sec. 2.3.4) is larger than 0.1%, 1.0%, and 10.0% [percent-per-square-degree](#) (calculated as the number of encountered convective events over the number of total released trajectories; on a 1° latitude × 1° longitude grid). (b) Same regions as in (a), but for all colored [regions-air masses](#) from Figs. 2-3. Background: OMI satellite measurements of the tropospheric NO₂ column, averaged over 14 days before the measurement. (c) Same as (b), but with density of convective events (as explained in Sec. 2.3.3) from TRACZILLA.

Table 2. Summary of air masses of interest marked with colored boxes (see Fig. 2), their altitude ranges, and local minima (↓) and maxima (↑) of trace gases measured by GLORIA (repeated from Sec. 3). Regions of origin, as indicated by ATLAS and TRACZILLA (see also Fig. 4) are listed. Approximate ages of air are shown in Supplementary Tab. 1.

<u>color</u>	<u>altitude</u>	<u>GLORIA measurements</u>	<u>ATLAS</u>	<u>TRACZILLA</u>
<u>red</u>	<u>15.75-16.75 km</u>	<u>HNO₃: 1.0 ppbv ↑</u> <u>PAN: >500 pptv ↑</u> <u>C₂H₂: 200 pptv ↑</u> <u>HCOOH: 150 pptv ↑</u>	<u>north eastern India,</u> <u>eastern China,</u> <u>central China</u>	<u>eastern China</u> <u>central China</u>
<u>magenta</u>	<u>14.5-15.75 km</u>	<u>HNO₃: 0.75 ppbv ↑</u> <u>PAN: 150 pptv ↓</u> <u>C₂H₂: 100 pptv ↓</u>	<u>eastern China,</u> <u>South China and</u> <u>Philippine Seas,</u> <u>north eastern</u> <u>India</u>	<u>eastern China,</u> <u>South China and</u> <u>Philippine Seas,</u> <u>Tibetan Plateau</u> <u>and Kashmir</u>
<u>orange</u>	<u>11.5-15.0 km</u>	<u>PAN: >500 pptv ↑</u> <u>C₂H₂: >200 pptv ↑</u> <u>HCOOH: >200 pptv ↑</u>	<u>eastern India,</u> <u>southern China,</u> <u>South China Sea</u>	<u>eastern India,</u> <u>southern China,</u> <u>South China Sea</u>
<u>blue</u>	<u>13.0-15.5 km</u>	<u>PAN: <150 pptv ↓</u> <u>C₂H₂: <80 pptv ↓</u> <u>HCOOH: <60 pptv ↓</u>	<u>Bay of Bengal,</u> <u>Myanmar,</u> <u>South China and</u> <u>Philippine Seas</u>	<u>Bay of Bengal,</u> <u>Myanmar,</u> <u>South China and</u> <u>Philippine Seas</u>
<u>purple</u>	<u>15.0-16.75 km</u>	<u>O₃: 400 ppbv ↑</u>	<u>eastern India,</u> <u>South China and</u> <u>Philippine Seas</u>	<u>eastern India,</u> <u>South China and</u> <u>Philippine Seas</u>
<u>cyan</u>	<u>16.0-18.5 km</u>	<u>PAN: 400 pptv ↑</u> <u>C₂H₂: 100 pptv ↑</u>	<u>South China and</u> <u>Philippine Seas,</u> <u>central China</u>	<u>South China and</u> <u>Philippine Seas</u>
<u>green</u>	<u>12.0-14.75 km</u>	<u>HCOOH: <20 pptv ↓</u>	<u>Tibetan Plateau,</u> <u>Kashmir</u>	<u>Tibetan Plateau,</u> <u>Kashmir</u>

The ATLAS and TRACZILLA models show partly different areas of convective events for the labeled regions-air masses of interest. A summary is given in Tab. 2. In the following parts, the plausibility of the calculated areas of convective events is tested by comparing these regions to the OMI NO₂ tropospheric column:

- The red region-air mass of interest has been selected ~~from the measurements~~ due to enhanced pollution trace gas and HNO₃ measurements during the first part of the flight, ~~in contrast to the magenta region, which showed enhanced HNO₃, but otherwise a local minimum of pollutant species.~~ For ATLAS and TRACZILLA, it was shown that only a small part of the trajectories experienced convection during 5 days before the measurement (see Fig. 3). In Fig. 4b-c, for both models

regions are marked red between the location of the measurement and eastern China. ~~As for most marked regions only the 0, 1% lines are present, the~~ For most regions marked red, convective influence along the trajectories was weak, thus only the 0.1 percent-per-square-degree contours are present. However, ~~red marked regions in north eastern China match to the most regions marked red in northeastern China lie close to areas with~~ enhanced NO₂ measurements and possibly, so these regions may possibly have contributed to the measured enhanced pollution trace gases. For the ATLAS model, it is shown in ~~supplementary Supplementary~~ Fig. 12 that for ~~backward trajectories from the red region the red air mass,~~ less than 30% ~~convective events occurred in these marked regions~~ of all started trajectories experienced a convective event within 10 days before the measurement, showing the weak convective influence.

5

10

15

20

25

30

- The magenta ~~region air mass~~ of interest is connected to a local minimum of PAN, and C₂H₂ and HCOOH, and enhanced HNO₃, close to the ~~red maximum.~~ Both maximum of the pollutant species marked with the red box. Both trajectory models show similar regions than for red convective densities as for the red regions above China, and in addition above the Southern Chinese and Philippine Sea they also show substantial convective activity above the South China and Philippine Seas. TRACZILLA also indicates regions ~~north western of of~~ strong convection northwest of the flight path, while ATLAS indicates a region in north eastern India, close to the flight path. Again, for almost all these marked regions ~~only the 0, 1% lines are present, which again indicates a low convective influence of,~~ convective influence on the measured air masses was weak, thus only the 0.1 percent-per-square-degree lines are present. However, in ~~case of convective contributions to these air masses~~ this case, it is ~~more likely that~~ likely that convection in the regions above the ~~Southern Chinese and Philippine Sea contributed with~~ South China and Philippine Seas brought up clean maritime air. Enhanced HNO₃ concentrations within these air masses possibly result from reaction of lightning NO_x with OH to HNO₃ (see e.g., Schumann and Huntrieser, 2007).
- The origin of the green colored air mass has been already discussed by Höpfner et al. (2019) on basis of similar trajectory sets and visualizations. Here, also regions with densities of convective events as low as 0.1 percent-per-square-degree are shown, and regions larger than those described by Höpfner et al. (2019) are marked. However, still both trajectory models highlight regions of the Tibetan Plateau and Kashmir as possible sources of the green air masses of interest. While GLORIA HCOOH shows a local minimum, enhancements of C₂H₂, PAN, and NH₃ (not shown) are measured. This chemical composition of the green marked air masses makes an origin from the relatively clean Tibetan Plateau unlikely. In addition, Höpfner et al. (2019) connected a boundary layer maximum of NH₃ in the Kashmir region (measured by IASI) with these air masses, which makes this Kashmir region the most likely origin of the measured air masses marked green. A connection of the minimum of GLORIA HCOOH with IASI boundary layer measurements of HCOOH has been discussed in Sec.2.1.
- The second part of the flight has again a region an air mass with enhanced NMVOC measurements, marked with orange color. Both models indicate that the trajectories encountered convection not too far away from the flight path. Between the flight path and the coast, ~~even the 1 %~~ percent-per-square-degree, and for TRACZILLA ~~also even the 10 %~~ percent-per-square-degree convective density lines are visible. This region is connected to enhanced OMI NO₂ mea-

measurements, which is a strong indication for local emissions from India. Smaller ~~orange regions~~ regions marked orange in both models, present above southern China and the ~~Southern Chinese~~ South China Sea, are not likely to contribute to the strongly enhanced measured pollutants. For the ATLAS model, it is shown in ~~supplementary~~ Supplementary Fig. 14 that for backward trajectories from the orange ~~region~~ air mass, about 50% of all convective events occur spatially very close to the measurement location and within 3 days before the measurement. This corresponds to the ~~more plausible~~ orange region (according to the orange region in India with enhanced NO₂ columns), which seems to be more likely to contribute to the measured air masses according to supplementary Fig. 14.

5

10

15

20

25

30

- A local minimum of NMVOCs at the same altitude of measurement as the ~~previous one~~ air mass outlined in orange is marked blue. Both models ~~indicates~~ indicate convective source regions between the flight path and the Bay of Bengal ~~as~~ source region, together with regions above Myanmar, and the South ~~Chinese and Philippine Sea~~ China and Philippine Seas. All these regions show low NO₂ ~~measurements~~ and are therefore plausible source regions for the rather clean air masses measured by GLORIA.
- The local maximum of O₃ in the second part of the flight ~~below the tropopause~~ is marked purple ~~in the measurements~~ (see Fig. 2). ~~According to~~ Based on the convection along the model trajectories, the origin of these air masses is very similar to that of the blue labeled air masses: Convection probabilities along the trajectories from the purple ~~region~~ air mass are enhanced over ~~west eastern~~ India and above the South Chinese and Philippine Sea. China and Philippine Seas. These areas marked by the trajectories show low OMI NO₂ and indicate relatively clean boundary layer air, which cannot explain the measured local enhancement of O₃. This suggests that the measured local maximum of O₃ is of other than convective origin; possibly, the measured maximum is a pollution remainder transported for more than 10 days, or an intrusion of stratospheric air.
- The cyan colored ~~regions~~ air masses are connected to the measured enhancement of PAN and C₂H₂ above the tropopause. In Sec. 3, it is suggested that these air masses are transported for more than a few days, ~~which indicates that convection 10 days before the measurement only had a minor influence to the transport of polluted air masses to the measurement geolocation~~ but for less than two weeks. For this reason, it is not expected to see strong convective influence on the trajectories a few days prior to the measurement. This is also supported by Fig. 3, which does not show ~~enhanced convection probability~~ strongly enhanced convection probabilities in the cross sections ~~for both trajectory models~~ for either trajectory model. ATLAS and TRACZILLA both only show a ~~region at~~ small convective region over the Philippine Sea for the cyan ~~region~~ air mass of interest, and ~~a region~~ ATLAS also shows convective activity above central China. For the ATLAS model, it is shown in ~~supplementary~~ Supplementary Fig. 17 that for backward trajectories from the cyan ~~region~~ air mass, less than 20% ~~convective events~~ of all trajectories ~~occurred at all~~ experienced any convective events, which also indicates the low convective influence.

In summary, both models suggest, that air masses of interest with enhanced pollution trace gas measurements (orange, red) originate from India or China, where boundary layer pollution is also observed by OMI. Air masses of interest with low

pollution trace gases measured are transported from maritime and pristine surface regions (blue). For air masses with low pollution trace gases, but locally enhanced O_3 or HNO_3 (magenta, purple), also maritime regions are indicated, which can explain low pollution trace gases, but not the enhanced O_3 or HNO_3 VMRs. As expected, the local maxima of PAN and C_2H_2 at altitudes of the tropopause (cyan) were transported for a longer time, according to the trajectory models. The origin of the local minima of HCOOH (green) already has been discussed to be most likely from the Kashmir region (Höpfner et al., 2019)

The comparison of ATLAS and TRACZILLA calculations of convective origin of the measured pollution species shows that there are few differences between these model results. Both models indicate regions of origin that are plausible source regions of pollutants, according to the give results for the source regions and convective age of air that are broadly consistent with the measurements. Due to the numerous uncertainties, there are, however, also some results which seem to be less plausible. However, OMI NO_2 measurements, while also both models indicate regions that are less plausible, which is shown as proxy for boundary layer pollution, does not account for biogenic sources and is shown as average over 14 days prior to the measurement (see Sec. 2.4). Due to these limitations, additional pollution sources may have been overlooked in this analysis. Still, similar origins of highly polluted air masses, indicated by two independent backward trajectory models, agree with enhanced surface pollution, measured by OMI. This agreement within the anticipated accuracy of the two backward trajectory models suggests that both models use reliable schemes for convection detection.

5 Comparison to model simulations

Another application of our highly resolved measurements is shown in this section, in the evaluation of atmospheric models. Simulation results of the CAMS reanalysis and EMAC atmospheric models are interpolated onto the geolocations of the GLORIA measurements (see Fig. 1). Comparisons with the GLORIA measurements for each gas are shown in Fig. 5. Due to the rather coarse horizontal resolution of the models, compared to the distance between GLORIA profiles, for these model comparisons the GLORIA cross sections for these model comparisons have been averaged over 33 single profiles, i.e. a horizontal distance of approx. 100 km.

Comparisons of GLORIA HNO_3 with CAMS (Fig. 5a-b) show that no noticeable enhancements are simulated by the CAMS model. HNO_3 data are provided in the CAMS reanalysis data product, but the model does not include stratospheric chemistry and thus no stratospheric HNO_3 . The comparison of the observations with EMAC HNO_3 (Fig. 5c) shows several similarities: High stratospheric VMRs up to 2 ppbv are simulated above 19 km of in the second part of the flight, that they decrease to values of 0.750.5 ppbv at the tropopause. Maximum Simulated maximum stratospheric values are not always simulated as high as the values measured, but agree they agree to within the GLORIA estimated error (see Supplement, Figs. 1 and 2). Delicate Fine-scale structures around the tropopause in the measurements are not repeated reproduced by the model, which can be explained with by the lower horizontal resolution of EMAC. Below the tropopause, the diagonal structure in the first part of the flight (of which parts are in the magenta box) are red and magenta boxes) is reproduced by EMAC. In the model, this structure continues into the second part of the flight, which has not been observed by GLORIA. This diagonal structure

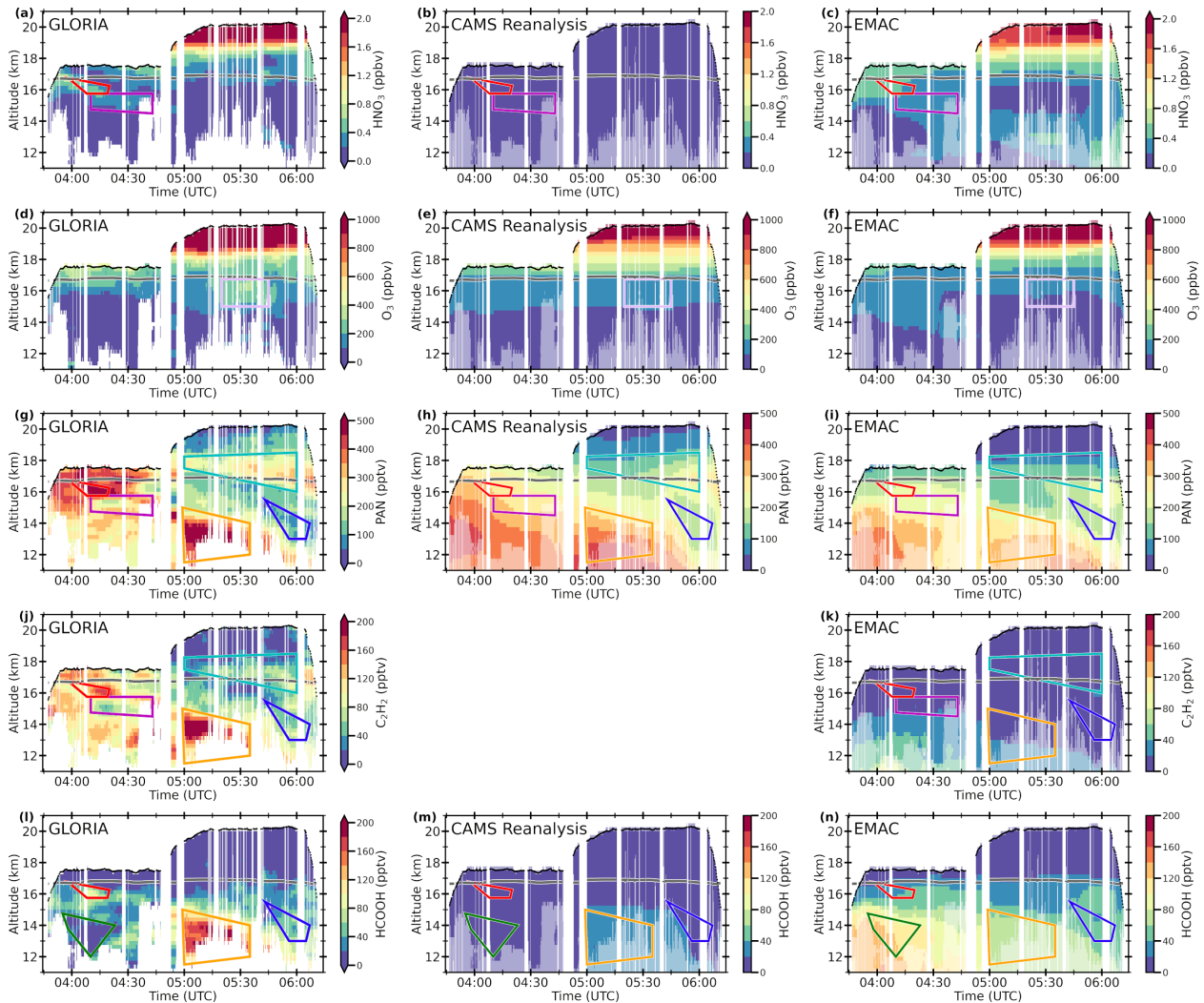


Figure 5. GLORIA (left column, similar to Fig. 2, but averaged over 33 single profiles), CAMS (middle column), and EMAC (right column) distributions of (a-c) HNO_3 , (d-f) O_3 , (g-i) PAN, (j-k) C_2H_2 , (l-n) HCOOH for StratoClim flight on 31 July 2017. CAMS reanalysis does not include C_2H_2 . All auxiliary lines as defined in the caption of Fig. 2. Altitudes not measured by GLORIA are marked with a white shadow in the model data.

coincides with the gradient of EMAC PAN (see below), which suggests that this simulated tropospheric HNO_3 originates from reactions with NO_2 , a product of the photolysis of PAN. ~~Too high values below the tropopause are also simulated towards the end of the flight (6:00 UTC). The difference in this diagonal structure between GLORIA and EMAC in the second part of the flight may result from a spatial displacement of the whole structure in the model, which is, however, unlikely due to the agreement of this HNO_3 structure in the first part of the flight, and due to the agreement of structures in pollution trace gases~~

in the second part of the flight (see below). It is more likely that EMAC overestimates the production of or underestimates the loss of HNO₃ here at altitudes below 14 km.

Comparisons between GLORIA O₃ and CAMS (Fig. 5d-e) show a general agreement between the two cross sections. In contrast to HNO₃, CAMS ~~does have~~ has reasonable stratospheric values for O₃ due to a satellite data assimilation scheme, which is only used for O₃ (Inness et al., 2015). The general distribution of O₃ is also well reproduced by the EMAC model, which does not assimilate satellite data, but applies a stratospheric chemistry scheme. Both models have difficulties ~~to simulate~~ in simulating the measured local enhancement at 5:30 UTC (purple box).

PAN is simulated similarly by CAMS and EMAC, and thus both models appear to have similar achievements and problems in reproducing the GLORIA measurements (Fig. 5g-i). The first part of the flight shows a local maximum (red box) above a local minimum (magenta box), ~~which is not~~ neither of which are simulated. Both models instead simulate a, more or less, constant decrease ~~of in~~ PAN with altitude. In the second part of the flight, both models succeed ~~to reproduce~~ in reproducing the location of relative maxima (orange and cyan boxes) and of the minimum (blue box), but not the absolute VMRs. While GLORIA measured more than 500 pptv of PAN in the orange box, CAMS simulates 400 pptv and EMAC not more than ~~300~~350 pptv. The background values of tropospheric PAN (blue box) are instead simulated higher (150 pptv) in CAMS and EMAC than measured (100 pptv). The measured enhancement above the tropopause (cyan box) is only visible in the models towards the end of the flight at approx. 1 km lower altitudes, and both models have lower maximum values (300 pptv for CAMS and 200 pptv for EMAC vs. ~~450~~350 pptv for GLORIA).

C₂H₂ is only simulated by EMAC, which shows VMRs below 75 pptv, ~~which is considerably below~~ considerably lower than the measured VMRs (Fig. 5j-k). In the first part of the flight, EMAC simulates enhancements of up to 50 pptv below 14 km, where also GLORIA measurements show a local maximum of up to 150 pptv C₂H₂. In the second part of the flight, again a very small enhancement at the tropopause at 6:00 UTC (cyan box) is visible in EMAC, which is at the same geolocation as the enhancement in the measurements, ~~but much weaker and less extensive. Measured maxima of C₂H₂ are not reproduced by the EMAC model.~~

For HCOOH (Fig. 5l-n), CAMS only simulates VMRs below 50 pptv, which are measured as background values by GLORIA. The spatial distribution in CAMS shows a tiny enhancement of up to 50 pptv close to the orange box, where GLORIA measured maximum values of more than 200 pptv. EMAC simulates HCOOH VMRs up to 125 pptv below 15 km altitude in the first part of the flight, where GLORIA measurements show no enhancements. The measured enhancement in the red box is not reproduced by the model, but a local maximum is simulated at the same altitudes later during this flight (at 4:30 UTC). In the second part of the flight, the measured maximum (orange box) is simulated as a local maximum, but with considerably lower VMRs ~~below of less than~~ 75 pptv. In the averaged GLORIA cross sections, a small local maximum of 60 pptv is visible after 6:00 UTC, which coincides with the small enhancement in EMAC.

These comparisons of GLORIA measurements with CAMS and EMAC show the limitations of atmospheric chemistry model simulations. In the first part of the flight, for all ~~other gases~~ gases other than HNO₃ in EMAC, not even the structure was correctly simulated. ~~This indicates that the meteorological fields which prescribe transport in the simulations, do not include the processes relevant for the observed situation. Other explanations for the observed discrepancies between models~~

and measurement are the source regions and emission strengths that are considered in the models. From Höpfner et al. (2019) it is known that air masses measured in this part of the flight have been influenced by convection over north-west India and northern Pakistan a few days before measurement. For that reason, a detailed analysis of trajectories is discussed in Sec. 4. In the second part of the flight, models typically succeed to reproduce in reproducing measured structures in the trace gases but with considerably lower absolute VMRs. This motivates the sensitivity study with EMAC in the next section, examining the influence of increased NMVOC emissions on the comparisons with GLORIA measurements. Further uncertainties in the models are errors within the concentrations of precursor species, uncertainties in or lack of implemented chemical reactions, temporal and spatial variability of the NMVOC emissions that are not considered by the emission inventories, and lack of or uncertainties in microphysical processes, such as scavenging.

6 Influence of increased NMVOC emissions

GLORIA (left column, repeated from Fig. 5, again averaged over 33 single profiles), EMAC with 50% (middle column), and EMAC with 100% increased NMVOC emissions (right column) distributions of (a-c) PAN, (d-f) C_2H_2 , (g-i) HCOOH for StratoClim flight on 31 July 2017. All auxiliary lines as defined in caption of Fig. 2. Altitudes not measured by GLORIA are marked with a white shadow in the model data.

In this section, the influence of increased NMVOC emissions as a possible source of uncertainty for the simulation results in the previous section is discussed for the EMAC model (see Fig. ??). Monks et al. (2018) suggest that NMVOC emissions are globally underestimated. As discussed in Sec. 5, it is expected that increased emissions improve the comparisons to GLORIA measurements in the peak VMRs and higher background VMRs. As shown in Fig. 3, both parts of the flight were under similar convective influence. Both models, CAMS and EMAC, and their driving meteorological fields are not expected to resolve all events of deep convection and therefore use parameterizations for convection. It may be possible that convective events responsible for pollution trace gas structures in the second part of the flight. During the first part of the flight, strong influence of convective events are suggested for altitudes up to 15 km. The comparison of this part of the flight is not expected to improve due to increased NMVOC emissions, and for that reason only the second part of the flight is discussed in detail here. As in the previous section, GLORIA results are presented as an average over 33 single profiles, to have comparable horizontal resolutions between measurement and model.

For PAN (Fig. ??a-c), the effect of increased NMVOC emissions is clearly visible in the comparison to the GLORIA measurements of the are better met by the model's meteorological fields and convection parameterizations than in the first part. For parameterizations of convection in EMAC, a large difference between different methods is reported for the upper troposphere (see Fig. 5, Tost et al., 2006). Other possible explanations of the observed discrepancies during the different flight parts are the source regions and emission strengths that are considered in the models. It is possible that source regions responsible for measured enhancements of pollutants in the second part of the flight. Simulation results of the emission scenario "+100%" successfully reproduce measured PAN VMRs of more than 500 pptv in the orange box and of 300 pptv in the cyan box. However, in both these simulations with increased emissions, PAN background VMRs between the local

maxima are too high in the simulation. E. g., in the blue box, more than 250 pptv (" +50%") and more than 350 pptv (" +100%") are simulated, while only less than 100 pptv are measured. are considered by the models, while the regions responsible for measured enhancements of pollutants in the first part of the flight are not.

In contrast to PAN, As a simple sensitivity test, we have increased NMVOC emissions in the EMAC model do not result in comparable C_2H_2 VMRs as in the measurement (Fig. ??d-f). In the orange box, more than 200 pptv of C_2H_2 are measured, while only less than 75 pptv are simulated in the " +100%" emission scenario. This is the same for enhancements at the tropopause (cyan box), where 100 pptv of C_2H_2 are simulated globally by 50%. This was motivated by Monks et al. (2018), who suggest that NMVOC emissions are globally underestimated. As expected, the new simulation results in Supplementary Fig. 20 have larger maximum VMRs of PAN, C_2H_2 are measured and only 50 pptv simulated towards the end of the flight.

The measured maximum of HCOOH of more than 200 pptv (orange box) is also not reproduced by the " +100%" emission scenario of the EMAC simulation, which only results in up to 125 pptv in the orange box (Fig. ??g-i). As already observed in the EMAC simulation without enhanced emissions (see Fig. 5n), an enhancement of HCOOH at 6:00 UTC and 16 km altitude becomes more visible with increasing emissions, which is not observed by GLORIA.

These comparisons of GLORIA measurements with EMAC simulations with increased NMVOC emissions show that for PAN, the increased NMVOC emissions improve the comparison of the simulated maximum values to the measurements. The measured maximum VMRs are better reproduced by EMAC with the " +100%" emission scenario. Anyhow, the tropospheric background values are modeled too high in both, the " +50%" and " +100%", simulation. This is possibly caused by the limited resolution of the EMAC results. The GLORIA observations have higher vertical resolutions compared to EMAC and thus are able to resolve strong vertical gradients that EMAC can only reproduce on average and therefore smooths the finer resolved image. The measured VMR distributions of C_2H_2 and HCOOH are not even reproduced by the EMAC run, and HCOOH, which in some cases match better to the GLORIA measurements. However, the overall structure in the trace gas distributions remains unchanged and still does not agree significantly better with 100% increased NMVOC emissions. This suggests that there are possibly other emission sources than in the emission inventory used by EMAC. Another explanation could be that emissions are not transported to the measurement geolocation as efficiently in the model as in reality. This also indicates convective events that are not resolved in the meteorological fields that are prescribing dynamics in EMAC. However, the overall structure of the simulated trace gases did not change due to the enhanced NMVOC emissions and therefore other uncertainties in the simulation (as discussed in Sec. 5) the observations. In addition, the background VMRs of PAN and HCOOH are considered to influence these structural differences between measurement and model considerably overestimated in the sensitivity run. This simple test indicates that other uncertainties in the model are more important for the mismatch to the GLORIA observations. These uncertainties in the models include errors in the concentrations of precursor species, uncertainties in or lack of implemented chemical reactions, temporal and spatial variability of the NMVOC emissions that are not considered by the emission inventories, and lack of or uncertainties in microphysical processes, such as scavenging. In addition, analyses of backward trajectories (see Supplementary Fig. 19 and Bucci et al., 2020) showed significantly different trajectory paths for ERA-Interim (used for the EMAC simulations) and ERA5. As shown by Bucci et al. (2020), ERA5 explains pollution features

better than does ERA-Interim. Based on these uncertainties, further model sensitivity studies are recommended to improve the agreement with the measurement, but are outside the scope of this study.

6 Conclusions

This study discusses the first simultaneous airborne measurements of HNO₃, O₃, PAN, C₂H₂, and HCOOH in high spatial resolution within the center of the AMA UTLS. The observations reveal ~~regions-air masses~~ with strongly enhanced mixing ratios of these pollutants with maximum VMRs of more than 500 pptv for PAN, and more than 200 pptv of C₂H₂ and HCOOH. In particular, a layer of enhanced PAN (≈ 400 pptv) and C₂H₂ (≈ 100 pptv) has been measured at and above the tropopause. From the atmospheric lifetimes and the trajectory analysis, it is estimated that these enhancements exist in the atmosphere for ~~longer-more~~ than a few days. Other air masses below 15 km ~~with strongly enhanced in which strongly enhanced concentrations~~ of pollution trace gases ~~measured-have been observed~~ are linked to recent convective events ~~as transport mechanism to the upper troposphere~~. These measurements and their analysis ~~show-confirm~~ that PAN, a precursor of O₃, is efficiently transported upwards by convection, and transported for a longer time in the tropopause region, as shown earlier by Glatthor et al. (2007), Fadnavis et al. (2015), and Ungermann et al. (2016). In contrast to the study by Gottschaldt et al. (2018), no enhancements of O₃ are visible in ~~our~~ the GLORIA measurements. However, the enhancements discussed by Gottschaldt et al. (2018) are within the estimated observational uncertainty and, thus, cannot be ruled out.

We found indications that HCOOH was washed out, while in the same air masses PAN, C₂H₂, and also water soluble NH₃ ~~was-were~~ transported to the measurement geolocation. ~~From-By~~ Höpfner et al. (2019), it is reported that a large amount of up to 1 ppbv of NH₃ was measured at-in the same air masses ~~of-as~~ the HCOOH minimum. Because IASI satellite total column measurements show ~~for both species, maxima for both~~ HCOOH and NH₃ maxima at the estimated area of origin of these air masses (according to Höpfner et al., 2019), it is suggested that the wash out process in ~~this-these~~ air masses was very different for ~~these-the two~~ species, due to their different Henry ~~constants's Law Constants~~ and the pH of the droplets. However, ~~we cannot rule out other processes leading to the different behavior other processes resulting in different UT transport characteristics of HCOOH and NH₃ upon transport to the UT, like a difference in retention of those gases upon freezing of the liquid water droplets at high altitudes (Ge et al., 2018). At later measurements NH₃ have been discussed by Ge et al. (2018). Later during~~ the flight, for air masses of different ~~origin and history~~ origins and histories, it is shown that enhanced HCOOH VMRs up to 200 pptv can reach altitudes up to 15 km without being washed out.

The analysis of backward trajectories from ATLAS and TRACZILLA shows that the two methods for the treatment of convection of these models highlight similar regions of enhanced convective upward transport. Backward trajectories, starting at the geolocations of measurements with local maxima and minima of NMVOCs, indicate various regions of enhanced convection and thus of the origin of these air masses. Air masses with enhanced PAN, C₂H₂, and HCOOH at altitudes between 12 and 15 km in the second part of the flight are connected with convection over India, while unpolluted air masses at similar altitudes are connected with convection events over sea and coastal areas. A comparison ~~of these indicated regions~~ with measured

OMI NO₂ enhancements ~~indicate~~ indicates that some of these regions are plausible pollution sources. Similarly to Bucci et al. (2020), we find a strong convective influence of the transport of polluted air masses to the upper troposphere.

Comparisons of the measurements to CAMS and EMAC simulation results show that the first part of the flight appears to be under high convective influence, which the models do not account for. In the second part of the flight, CAMS and EMAC reproduce large scale structures of the spatial distributions of the measured trace gases, while the simulated ~~VMRs peak VMRs of PAN, C₂H₂, and HCOOH~~ are considerably lower compared to the measurements. ~~We have performed a sensitivity study with EMAC with enhanced NMVOC emissions, increased by 50% and 100%. With the increased NMVOC emissions, the simulations show similar maximum values for PAN compared to GLORIA, but tropospheric background VMRs are simulated considerably too high. These too high background VMRs are attributed at least partly to the spatial resolution of EMAC, which does not resolve structures as fine as measured by GLORIA due to numerical diffusion in the model. EMAC simulations of C₂H₂ and HCOOH do not reproduce the strong enhancements in the second part of the flight, even with emissions increased by 100%. Therefore Tropospheric background VMRs instead are simulated too high for PAN and HCOOH (the latter only for EMAC). An EMAC sensitivity test with NMVOC emission globally increased by 50%, did not considerably improve the agreement between simulation and measurements. Therefore,~~ other uncertainties in the model apparently play a greater role: The emissions used in the model might not reproduce the temporal and spatial variability, convection events are not covered by the meteorological fields ~~and the or model parameterizations, and chemical processes in the model might be uncertain. In addition, the~~ T106 horizontal resolution still is rather ~~course~~ coarse for these highly resolved measurements by GLORIA.

In our paper, we show that there are very ~~delicate~~ fine-scale structures and a large variability of pollutant trace gases over horizontal scales of 200 km in the Asian monsoon UTLS. Some ~~enhancements~~ pollutants have been transported into the upper troposphere by convection within days before the measurements, while one ~~measured region has been transported around the tropopause and lowermost stratosphere~~ part of the observed air masses remained at UTLS altitudes for a longer time. Atmospheric models have difficulties in reproducing ~~these structures and explaining the origin of the measured species, which is likely to be caused by uncertainties of the~~ structures of the observed pollutant trace gas concentrations, likely because of uncertainties in the prescribed NMVOC emissions, rather coarse model resolution, and insufficient vertical transport from convection in ~~meteorological fields~~ the meteorological fields used to drive the model. Advanced schemes for convection detection along backward trajectories allow for ~~an estimation of origin for the identification of source regions of~~ the polluted air masses measured by GLORIA.

Data availability. GLORIA measurements are available in the database HALO-DB (<https://halo-db.pa.op.dlr.de/mission/101>) and will be available on the KITopen repository. The CAMS model data is available from ECMWF (<https://apps.ecmwf.int/data-catalogues/cams-reanalysis>).

30 OMI NO₂ level 3 data is available from NASA (<https://doi.org/10.5067/Aura/OMI/DATA3007> Krotkov, 2013). The EMAC, ATLAS, and TRACZILLA data are available upon request.

Author contributions. SJ initiated the study, performed the analyses, and wrote the manuscript. MH, JU, GW, NG, and SJ performed the GLORIA data processing. FFV and EK operated GLORIA during the StratoClim campaign in Kathmandu. OK performed the EMAC simulations and designed the sensitivity study. SB and BL performed the TRACZILLA trajectory simulations. IW performed the ATLAS trajectory simulations. All authors commented on and improved the manuscript.

5 *Competing interests.* The authors declare that they have no conflict of interest.

Acknowledgements. We gratefully thank the StratoClim coordination team, in particular Fred Stroh, and Myasishchev Design Bureau for successfully conducting the field campaign. The results are based on the efforts of all members of the GLORIA team, including the technology institutes ZEA-1 and ZEA-2 at Forschungszentrum Jülich and the Institute for Data Processing and Electronics at the Karlsruhe Institute of Technology. We thank ECMWF for providing CAMS data and NASA for providing OMI data. The EMAC simulations were performed on
10 the supercomputer ForHLR funded by the Ministry of Science, Research and the Arts Baden-Württemberg and by the Federal Ministry of Education and Research. [We thank Michelle Santee and one anonymous referee for improving this manuscript during the review process.](#)
[We gratefully acknowledge support by the translation services at Karlsruhe Institute of Technology.](#)

Sören Johansson has received funding from the European Community's Seventh Framework Programme (FP7/2007–2013) under grant agreement 603557. We acknowledge support by the Deutsche Forschungsgemeinschaft and the Open Access Publishing Fund of the Karl-
15 sruhe Institute of Technology.

References

- Bian, J., Pan, L. L., Paulik, L., Vömel, H., Chen, H., and Lu, D.: In situ water vapor and ozone measurements in Lhasa and Kunming during the Asian summer monsoon, *Geophysical Research Letters*, 39, <https://doi.org/10.1029/2012GL052996>, <https://agupubs.onlinelibrary.wiley.com/doi/pdf/10.1029/2012GL052996>, 2012.
- 5 Boursoukidis, E., Helleis, F., Tomsche, L., Fischer, H., Hofmann, R., Lelieveld, J., and Williams, J.: An aircraft gas chromatograph–mass spectrometer System for Organic Fast Identification Analysis (SOFIA): design, performance and a case study of Asian monsoon pollution outflow, *Atmospheric Measurement Techniques*, 10, 5089–5105, <https://doi.org/10.5194/amt-10-5089-2017>, <https://amt.copernicus.org/articles/10/5089/2017/amt-10-5089-2017-relations.html>, 2017.
- Bozem, H., Butler, T. M., Lawrence, M. G., Harder, H., Martinez, M., Kubistin, D., Lelieveld, J., and Fischer, H.: Chemical processes related to net ozone tendencies in the free troposphere, *Atmospheric Chemistry and Physics*, 17, 10 565–10 582, <https://doi.org/10.5194/acp-17-10565-2017>, 2017.
- Brasseur, G. and Solomon, S.: *Aeronomy of the middle atmosphere: Chemistry and physics of the stratosphere and mesosphere*, vol. 32 of *Atmospheric and oceanographic sciences library*, Springer, Dordrecht and [Great Britain], 3rd rev. and enl. edn., 2005.
- Braun, M., Grooß, J.-U., Woiwode, W., Johansson, S., Höpfner, M., Friedl-Vallon, F., Oelhaf, H., Preusse, P., Ungermann, J., Sinnhuber, B.-M., Ziereis, H., and Braesicke, P.: Nitrification of the lowermost stratosphere during the exceptionally cold Arctic winter 2015–2016, *Atmospheric Chemistry and Physics*, 19, 13 681–13 699, <https://doi.org/10.5194/acp-19-13681-2019>, <https://www.atmos-chem-phys.net/19/13681/2019/acp-19-13681-2019.pdf>, 2019.
- 15 Browell, E. V., Danielsen, E. F., Ismail, S., Gregory, G. L., and Beck, S. M.: Tropopause fold structure determined from airborne lidar and in situ measurements, *Journal of Geophysical Research*, 92, 2112, <https://doi.org/10.1029/JD092iD02p02112>, 1987.
- 20 Brunamonti, S., Jorge, T., Oelsner, P., Hanumanthu, S., Singh, B. B., Kumar, K. R., Sonbawne, S., Meier, S., Singh, D., Wienhold, F. G., Luo, B. P., Boettcher, M., Poltera, Y., Jauhiainen, H., Kayastha, R., Karmacharya, J., Dirksen, R., Naja, M., Rex, M., Fadnavis, S., and Peter, T.: Balloon-borne measurements of temperature, water vapor, ozone and aerosol backscatter on the southern slopes of the Himalayas during StratoClim 2016–2017, *Atmospheric Chemistry and Physics*, 18, 15 937–15 957, <https://doi.org/10.5194/acp-18-15937-2018>, <https://www.atmos-chem-phys.net/18/15937/2018/acp-18-15937-2018.pdf>, 2018.
- 25 Bucci, S., Legras, B., Sellitto, P., D’Amato, F., Viciani, S., Montori, A., Chiarugi, A., Ravegnani, F., Ulanovsky, A., Cairo, F., and Stroh, F.: Deep convective influence on the UTLS composition in the Asian Monsoon Anticyclone region: 2017 StratoClim campaign results, *Atmospheric Chemistry and Physics Discussions*, pp. 1–29, <https://doi.org/10.5194/acp-2019-1053>, <https://www.atmos-chem-phys-discuss.net/acp-2019-1053/acp-2019-1053.pdf>, 2020.
- Burkholder, J. B., Sander, S. P., Abbatt, J., Barker, J. R., Huie, R. E., Kolb, C. E., Kurylo, M. J., Orkin, V. L., Wilmouth, D. M., and Wine, P. H.: *Chemical Kinetics and Photochemical Data for Use in Atmospheric Studies*, Evaluation No. 18, JPL Publication, 15-10, <http://jpldataeval.jpl.nasa.gov>, 2015.
- 30 Coheur, P.-F., Herbin, H., Clerbaux, C., Hurtmans, D., Wespes, C., Carleer, M., Turquety, S., Rinsland, C. P., Remedios, J., Hauglustaine, D., Boone, C. D., and Bernath, P. F.: ACE-FTS observation of a young biomass burning plume: First reported measurements of C₂H₄, C₃H₆O, H₂CO and PAN by infrared occultation from space, *Atmospheric Chemistry and Physics*, 7, 5437–5446, <https://doi.org/10.5194/acp-7-5437-2007>, <https://www.atmos-chem-phys.net/7/5437/2007/acp-7-5437-2007.pdf>, 2007.
- 35

- Coheur, P.-F., Clarisse, L., Turquety, S., Hurtmans, D., and Clerbaux, C.: IASI measurements of reactive trace species in biomass burning plumes, *Atmospheric Chemistry and Physics*, 9, 5655–5667, <https://doi.org/10.5194/acp-9-5655-2009>, <https://www.atmos-chem-phys.net/9/5655/2009/acp-9-5655-2009.pdf>, 2009.
- Crutzen, P. J.: The role of NO and NO₂ in the chemistry of the troposphere and stratosphere, *Annual review of earth and planetary sciences*, 7, 443–472, 1979.
- Cussac, M., Marécal, V., Thouret, V., Josse, B., and Sauvage, B.: The impact of biomass burning on upper tropospheric carbon monoxide: a study using MOCAGE global model and IAGOS airborne data, *Atmospheric Chemistry and Physics*, 20, 9393–9417, <https://doi.org/10.5194/acp-20-9393-2020>, <https://acp.copernicus.org/articles/20/9393/2020/>, 2020.
- Dee, D. P., Uppala, S. M., Simmons, A. J., Berrisford, P., Poli, P., Kobayashi, S., Andrae, U., Balmaseda, M. A., Balsamo, G., Bauer, P., Bechtold, P., Beljaars, A. C. M., van de Berg, L., Bidlot, J., Bormann, N., Delsol, C., Dragani, R., Fuentes, M., Geer, A. J., Haimberger, L., Healy, S. B., Hersbach, H., Hólm, E. V., Isaksen, L., Kållberg, P., Köhler, M., Matricardi, M., McNally, A. P., Monge-Sanz, B. M., Morcrette, J., Park, B., Peubey, C., Rosnay, P. d., Tavolato, C., Thépaut, J., and Vitart, F.: The ERA-Interim reanalysis: configuration and performance of the data assimilation system, *Quarterly Journal of the Royal Meteorological Society*, 137, 553–597, <https://doi.org/10.1002/qj.828>, <https://rmets.onlinelibrary.wiley.com/doi/pdf/10.1002/qj.828>, 2011.
- Derrien, M., Le Gleau, H., and Raoul, M.-P.: The use of the high resolution visible in SAFNWC/MSG cloud mask, <https://hal-meteofrance.archives-ouvertes.fr/meteo-00604325/document>, 2010.
- Eyring, V., Lamarque, J.-F., Hess, P., Arfeuille, F., Bowman, K., Chipperfield, M., Duncan, B., Fiore, A., Gettelman, A., Giorgetta, M., Granier, C., Hegglin, M., Kinnison, D., Kunze, M., Langematz, U., Luo, B., Martin, R., Matthes, K., Newman, P., Peter, T., Robock, A., Ryerson, A., Saiz-Lopez, A., Salawitch, R., Schultz, M., Shepherd, T., Shindell, D., Stählerin, J., Tegtmeier, S., Thomason, L., Tilmes, S., Vernier, J.-P., Waugh, D., and Young, P.: Overview of IGAC/SPARC Chemistry-Climate Model Initiative (CCMI) Community Simulations in Support of Upcoming Ozone and Climate Assessments, *SPARC Newsletter*, 40, <http://www.sparc-climate.org/publications/newsletter/>, 2013.
- Fadnavis, S., Schultz, M. G., Semeniuk, K., Mahajan, A. S., Pozzoli, L., Sonbawne, S., Ghude, S. D., Kiefer, M., and Eckert, E.: Trends in peroxyacetyl nitrate (PAN) in the upper troposphere and lower stratosphere over southern Asia during the summer monsoon season: regional impacts, *Atmospheric Chemistry and Physics*, 14, 12 725–12 743, <https://doi.org/10.5194/acp-14-12725-2014>, 2014.
- Fadnavis, S., Semeniuk, K., Schultz, M. G., Kiefer, M., Mahajan, A., Pozzoli, L., and Sonbawane, S.: Transport pathways of peroxyacetyl nitrate in the upper troposphere and lower stratosphere from different monsoon systems during the summer monsoon season, *Atmospheric Chemistry and Physics*, 15, 11 477–11 499, <https://doi.org/10.5194/acp-15-11477-2015>, <https://www.atmos-chem-phys.net/15/11477/2015/>, 2015.
- Fischer, E. V., Jacob, D. J., Yantosca, R. M., Sulprizio, M. P., Millet, D. B., Mao, J., Paulot, F., Singh, H. B., Roiger, A., Ries, L., Talbot, R. W., Dzepina, K., and Pandey Deolal, S.: Atmospheric peroxyacetyl nitrate (PAN): A global budget and source attribution, *Atmospheric Chemistry and Physics*, 14, 2679–2698, <https://doi.org/10.5194/acp-14-2679-2014>, <https://www.atmos-chem-phys.net/14/2679/2014/acp-14-2679-2014.pdf>, 2014.
- Flemming, J., Huijnen, V., Arteta, J., Bechtold, P., Beljaars, A., Blechschmidt, A.-M., Diamantakis, M., Engelen, R. J., Gaudel, A., Inness, A., Jones, L., Josse, B., Katragkou, E., Marecal, V., Peuch, V.-H., Richter, A., Schultz, M. G., Stein, O., and Tsikerdekis, A.: Tropospheric chemistry in the Integrated Forecasting System of ECMWF, *Geoscientific Model Development*, 8, 975–1003, <https://doi.org/10.5194/gmd-8-975-2015>, <https://www.geosci-model-dev.net/8/975/2015/gmd-8-975-2015.pdf>, 2015.

- Friedl-Vallon, F., Gulde, T., Hase, F., Kleinert, A., Kulesa, T., Maucher, G., Neubert, T., Olschewski, F., Piesch, C., Preusse, P., Rongen, H., Sartorius, C., Schneider, H., Schönfeld, A., Tan, V., Bayer, N., Blank, J., Dapp, R., Ebersoldt, A., Fischer, H., Graf, F., Guggenmoser, T., Höpfner, M., Kaufmann, M., Kretschmer, E., Latzko, T., Nordmeyer, H., Oelhaf, H., Orphal, J., Riese, M., Schardt, G., Schillings, J., Sha, M. K., Suminska-Ebersoldt, O., and Ungermann, J.: Instrument concept of the imaging Fourier transform spectrometer GLORIA, *Atmospheric Measurement Techniques*, 7, 3565–3577, <https://doi.org/10.5194/amt-7-3565-2014>, 2014.
- 5 Froidevaux, L., Waters, J. W., Read, W. G., Elson, L. S., Flower, D. A., and Jarnot, R. F.: Global Ozone Observations from the UARS MLS: An Overview of Zonal-Mean Results, *Journal of the Atmospheric Sciences*, 51, 2846–2866, [https://doi.org/10.1175/1520-0469\(1994\)051<2846:GOOFTM>2.0.CO;2](https://doi.org/10.1175/1520-0469(1994)051<2846:GOOFTM>2.0.CO;2), 1994.
- Fujino, J., Nair, R., Kainuma, M., Masui, T., and Matsuoka, Y.: Multi-gas Mitigation Analysis on Stabilization Scenarios Using Aim Global Model, *The Energy Journal*, SI2006, <https://doi.org/10.5547/ISSN0195-6574-EJ-VolSI2006-NoSI3-17>, 2006.
- 10 Ge, C., Zhu, C., Francisco, J. S., Zeng, X. C., and Wang, J.: A molecular perspective for global modeling of upper atmospheric NH₃ from freezing clouds, *Proceedings of the National Academy of Sciences*, 115, 6147–6152, <https://doi.org/10.1073/pnas.1719949115>, <https://www.pnas.org/content/115/24/6147>, 2018.
- Glatthor, N., von Clarmann, T., Fischer, H., Funke, B., Grabowski, U., Höpfner, M., Kellmann, S., Kiefer, M., Linden, A., Milz, M., Steck, T., 15 and Stiller, G. P.: Global peroxyacetyl nitrate (PAN) retrieval in the upper troposphere from limb emission spectra of the Michelson Interferometer for Passive Atmospheric Sounding (MIPAS), *Atmospheric Chemistry and Physics*, 7, 2775–2787, <https://doi.org/10.5194/acp-7-2775-2007>, <https://www.atmos-chem-phys.net/7/2775/2007/acp-7-2775-2007.pdf>, 2007.
- Gottschaldt, K.-D., Schlager, H., Baumann, R., Bozem, H., Eyring, V., Hoor, P., Jöckel, P., Jurkat, T., Voigt, C., Zahn, A., and Ziereis, H.: Trace gas composition in the Asian summer monsoon anticyclone: a case study based on aircraft observations and model simulations, 20 *Atmospheric Chemistry and Physics*, 17, 6091–6111, <https://doi.org/10.5194/acp-17-6091-2017>, 2017.
- Gottschaldt, K.-D., Schlager, H., Baumann, R., Cai, D. S., Eyring, V., Graf, P., Grewe, V., Jöckel, P., Jurkat-Witschas, T., Voigt, C., Zahn, A., and Ziereis, H.: Dynamics and composition of the Asian summer monsoon anticyclone, *Atmospheric Chemistry and Physics*, 18, 5655–5675, <https://doi.org/10.5194/acp-18-5655-2018>, <https://www.atmos-chem-phys.net/18/5655/2018/acp-18-5655-2018.pdf>, 2018.
- Granier, C., Bessagnet, B., Bond, T., D’Angiola, A., van der Denier Gon, H., Frost, G. J., Heil, A., Kaiser, J. W., Kinne, S., Klimont, Z., 25 Kloster, S., Lamarque, J.-F., Lioussé, C., Masui, T., Meleux, F., Mieville, A., Ohara, T., Raut, J.-C., Riahi, K., Schultz, M. G., Smith, S. J., Thompson, A., van Aardenne, J., van der Werf, G. R., and van Vuuren, D. P.: Evolution of anthropogenic and biomass burning emissions of air pollutants at global and regional scales during the 1980–2010 period, *Climatic Change*, 109, 163–190, <https://doi.org/10.1007/s10584-011-0154-1>, 2011.
- Grutter, M., Glatthor, N., Stiller, G. P., Fischer, H., Grabowski, U., Höpfner, M., Kellmann, S., Linden, A., and von Clarmann, T.: Global distribution and variability of formic acid as observed by MIPAS-ENVISAT, *Journal of Geophysical Research: Atmospheres*, 115, <https://doi.org/10.1029/2009JD012980>, <https://agupubs.onlinelibrary.wiley.com/doi/full/10.1029/2009JD012980>, 2010.
- Guenther, A. B., Jiang, X., Heald, C. L., Sakulyanontvittaya, T., Duhl, T., Emmons, L. K., and Wang, X.: The Model of Emissions of Gases and Aerosols from Nature version 2.1 (MEGAN2.1): an extended and updated framework for modeling biogenic emissions, *Geoscientific Model Development*, 5, 1471–1492, <https://doi.org/10.5194/gmd-5-1471-2012>, <https://gmd.copernicus.org/articles/5/1471/2012/>, 2012.
- 35 Hoyle, C. R., Marécal, V., Russo, M. R., Allen, G., Arteta, J., Chemel, C., Chipperfield, M. P., D’Amato, F., Dessens, O., Feng, W., Hamilton, J. F., Harris, N. R. P., Hosking, J. S., Lewis, A. C., Morgenstern, O., Peter, T., Pyle, J. A., Reddman, T., Richards, N. A. D., Telford, P. J., Tian, W., Viciani, S., Volz-Thomas, A., Wild, O., Yang, X., and Zeng, G.: Representation of tropical deep convection in atmospheric models – Part 2: Tracer transport, *Atmospheric Chemistry and Physics*, 11, 8103–8131, <https://doi.org/10.5194/acp-11-8103-2011>, 2011.

- Höpfner, M., Volkamer, R., Grabowski, U., Grutter, M., Orphal, J., Stiller, G., Clarmann, T. V., and Wetzel, G.: First detection of ammonia (NH₃) in the Asian summer monsoon upper troposphere, *Atmospheric Chemistry and Physics*, 16, 14357–14369, <https://doi.org/10.5194/acp-16-14357-2016>, <https://www.atmos-chem-phys.net/16/14357/2016/acp-16-14357-2016.pdf>, 2016.
- Höpfner, M., Ungermann, J., Borrmann, S., Wagner, R., Spang, R., Riese, M., Stiller, G., Appel, O., Batenburg, A. M., Bucci, S., Cairo, F., Dragoneas, A., Friedl-Vallon, F., Hünig, A., Johansson, S., Krasauskas, L., Legras, B., Leisner, T., Mahnke, C., Möhler, O., Mollerker, S., Müller, R., Neubert, T., Orphal, J., Preusse, P., Rex, M., Saathoff, H., Strohm, F., Weigel, R., and Wohltmann, I.: Ammonium nitrate particles formed in upper troposphere from ground ammonia sources during Asian monsoons, *Nature Geoscience*, 12, 608–612, <https://doi.org/10.1038/s41561-019-0385-8>, 2019.
- Inness, A., Blechschmidt, A.-M., Bouarar, I., Chabrillat, S., Crepulja, M., Engelen, R. J., Eskes, H., Flemming, J., Gaudel, A., Hendrick, F., Huijnen, V., Jones, L., Kapsomenakis, J., Katragkou, E., Keppens, A., Langerock, B., Mazière, M. D., Melas, D., Parrington, M., Peuch, V. H., Razinger, M., Richter, A., Schultz, M. G., Suttie, M., Thouret, V., Vrekoussis, M., Wagner, A., and Zerefos, C.: Data assimilation of satellite-retrieved ozone, carbon monoxide and nitrogen dioxide with ECMWF's Composition-IFS, *Atmospheric Chemistry and Physics*, 15, 5275–5303, <https://doi.org/10.5194/acp-15-5275-2015>, <https://www.atmos-chem-phys.net/15/5275/2015/>, 2015.
- Inness, A., Ades, M., Agustí-Panareda, A., Barré, J., Benedictow, A., Blechschmidt, A.-M., Dominguez, J. J., Engelen, R., Eskes, H., Flemming, J., Huijnen, V., Jones, L., Kipling, Z., Massart, S., Parrington, M., Peuch, V.-H., Razinger, M., Remy, S., Schulz, M., and Suttie, M.: The CAMS reanalysis of atmospheric composition, *Atmospheric Chemistry and Physics*, 19, 3515–3556, <https://doi.org/10.5194/acp-19-3515-2019>, <https://www.atmos-chem-phys.net/19/3515/2019/acp-19-3515-2019.pdf>, 2019.
- James, R., Bonazzola, M., Legras, B., Surbled, K., and Fueglistaler, S.: Water vapor transport and dehydration above convective outflow during Asian monsoon, *Geophysical Research Letters*, 35, <https://doi.org/10.1029/2008GL035441>, <https://agupubs.onlinelibrary.wiley.com/doi/pdf/10.1029/2008GL035441>, 2008.
- Jöckel, P., Kerkweg, A., Pozzer, A., Sander, R., Tost, H., Riede, H., Baumgaertner, A., Gromov, S., and Kern, B.: Development cycle 2 of the Modular Earth Submodel System (MESSy2), *Geoscientific Model Development*, 3, 717–752, <https://doi.org/10.5194/gmd-3-717-2010>, <https://www.geosci-model-dev.net/3/717/2010/gmd-3-717-2010.pdf>, 2010.
- Jöckel, P., Tost, H., Pozzer, A., Kunze, M., Kirner, O., Brenninkmeijer, C. A. M., Brinkop, S., Cai, D. S., Dyroff, C., Eckstein, J., Frank, F., Garny, H., Gottschaldt, K.-D., Graf, P., Grewe, V., Kerkweg, A., Kern, B., Matthes, S., Mertens, M., Meul, S., Neumaier, M., Nützel, M., Oberländer-Hayn, S., Ruhnke, R., Runde, T., Sander, R., Scharffe, D., and Zahn, A.: Earth System Chemistry integrated Modelling (ESCiMo) with the Modular Earth Submodel System (MESSy) version 2.51, *Geoscientific Model Development*, 9, 1153–1200, <https://doi.org/10.5194/gmd-9-1153-2016>, 2016.
- Johansson, S., Woiwode, W., Höpfner, M., Friedl-Vallon, F., Kleinert, A., Kretschmer, E., Latzko, T., Orphal, J., Preusse, P., Ungermann, J., Santee, M. L., Jurkat-Witschas, T., Marsing, A., Voigt, C., Giez, A., Krämer, M., Rolf, C., Zahn, A., Engel, A., Sinnhuber, B.-M., and Oelhaf, H.: Airborne limb-imaging measurements of temperature, HNO₃, O₃, ClONO₂, H₂O and CFC-12 during the Arctic winter 2015/2016: Characterization, in situ validation and comparison to Aura/MLS, *Atmospheric Measurement Techniques*, 11, 4737–4756, <https://doi.org/10.5194/amt-11-4737-2018>, <https://www.atmos-meas-tech.net/11/4737/2018/amt-11-4737-2018.pdf>, 2018.
- Jurkat, T., Kaufmann, S., Voigt, C., Schäuble, D., Jeßberger, P., and Ziereis, H.: The airborne mass spectrometer AIMS – Part 2: Measurements of trace gases with stratospheric or tropospheric origin in the UTLS, *Atmospheric Measurement Techniques*, 9, 1907–1923, <https://doi.org/10.5194/amt-9-1907-2016>, <https://www.atmos-meas-tech.net/9/1907/2016/amt-9-1907-2016.pdf>, 2016.

- Kaiser, J. W., Heil, A., Andreae, M. O., Benedetti, A., Chubarova, N., Jones, L., Morcrette, J.-J., Razinger, M., Schultz, M. G., Suttie, M., and van der Werf, G. R.: Biomass burning emissions estimated with a global fire assimilation system based on observed fire radiative power, *Biogeosciences*, 9, 527–554, <https://doi.org/10.5194/bg-9-527-2012>, <https://bg.copernicus.org/articles/9/527/2012/>, 2012.
- 5 Krotkov, N. A.: OMI/Aura NO₂ Cloud-Screened Total and Tropospheric Column Daily L3 Global 0.25deg Lat/Lon Grid, <https://doi.org/10.5067/AURA/OMI/DATA3007>, 2013.
- Krotkov, N. A., Lamsal, L. N., Celarier, E. A., Swartz, W. H., Marchenko, S. V., Bucsela, E. J., Chan, K. L., Wenig, M., and Zara, M.: The version 3 OMI NO₂ standard product, *Atmospheric Measurement Techniques*, 10, 3133–3149, <https://doi.org/10.5194/amt-10-3133-2017>, 2017.
- Lamarque, J.-F., Dentener, F., McConnell, J., Ro, C.-U., Shaw, M., Vet, R., Bergmann, D., Cameron-Smith, P., Dalsoren, S., Doherty, R., Faluvegi, G., Ghan, S. J., Josse, B., Lee, Y. H., MacKenzie, I. A., Plummer, D., Shindell, D. T., Skeie, R. B., Stevenson, D. S., Strode, S., Zeng, G., Curran, M., Dahl-Jensen, D., Das, S., Fritzsche, D., and Nolan, M.: Multi-model mean nitrogen and sulfur deposition from the Atmospheric Chemistry and Climate Model Intercomparison Project (ACCMIP): evaluation of historical and projected future changes, *Atmospheric Chemistry and Physics*, 13, 7997–8018, <https://doi.org/10.5194/acp-13-7997-2013>, <https://acp.copernicus.org/articles/13/7997/2013/>, 2013.
- 10 Legras, B. and Bucci, S.: Confinement of air in the Asian monsoon anticyclone and pathways of convective air to the stratosphere during summer season, *Atmospheric Chemistry and Physics Discussions*, pp. 1–37, <https://doi.org/10.5194/acp-2019-1075>, <https://www.atmos-chem-phys-discuss.net/acp-2019-1075/acp-2019-1075.pdf>, 2019.
- Legras, B., Pisso, I., Berthet, G., and Lefèvre, F.: Variability of the Lagrangian turbulent diffusion in the lower stratosphere, *Atmospheric Chemistry and Physics*, 5, 1605–1622, <https://doi.org/10.5194/acp-5-1605-2005>, <https://www.atmos-chem-phys.net/5/1605/2005/acp-5-1605-2005.pdf>, 2005.
- 20 Lelieveld, J., Bourtsoukidis, E., Brühl, C., Fischer, H., Fuchs, H., Harder, H., Hofzumahaus, A., Holland, F., Marno, D., Neumaier, M., Pozzer, A., Schlager, H., Williams, J., Zahn, A., and Ziereis, H.: The South Asian monsoon—pollution pump and purifier, *Science*, 361, 270–273, <https://doi.org/10.1126/science.aar2501>, <https://science.sciencemag.org/content/sci/361/6399/270.full.pdf>, 2018.
- Levelt, P. F., van den Oord, G., Dobber, M. R., Malkki, A., Visser, H., Vries, J. d., Stammes, P., Lundell, J., and Saari, H.: The ozone monitoring instrument, *IEEE Transactions on Geoscience and Remote Sensing*, 44, 1093–1101, <https://doi.org/10.1109/TGRS.2006.872333>, 2006.
- 25 Li, D., Vogel, B., Müller, R., Bian, J., Günther, G., Li, Q., Zhang, J., Bai, Z., Vömel, H., and Riese, M.: High tropospheric ozone in Lhasa within the Asian summer monsoon anticyclone in 2013: influence of convective transport and stratospheric intrusions, *Atmospheric Chemistry and Physics*, 18, 17 979–17 994, <https://doi.org/10.5194/acp-18-17979-2018>, <https://www.atmos-chem-phys.net/18/17979/2018/acp-18-17979-2018.pdf>, 2018.
- 30 Livesey, N. J., Filipiak, M. J., Froidevaux, L., Read, W. G., Lambert, A., Santee, M. L., Jiang, J. H., Pumphrey, H. C., Waters, J. W., Cofield, R. E., Cuddy, D. T., Daffer, W. H., Drouin, B. J., Fuller, R. A., Jarnot, R. F., Jiang, Y. B., Knosp, B. W., Li, Q. B., Perun, V. S., Schwartz, M. J., Snyder, W. V., Stek, P. C., Thurstans, R. P., Wagner, P. A., Avery, M., Browell, E. V., Cammas, J., Christensen, L. E., Diskin, G. S., Gao, R., Jost, H., Loewenstein, M., Lopez, J. D., Nedelec, P., Osterman, G. B., Sachse, G. W., and Webster, C. R.: Validation of Aura Microwave Limb Sounder O₃ and CO observations in the upper troposphere and lower stratosphere, *Journal of Geophysical Research: Atmospheres*, 113, <https://doi.org/10.1029/2007JD008805>, <https://agupubs.onlinelibrary.wiley.com/doi/full/10.1029/2007JD008805>, 2008.

- Meinshausen, M., Smith, S. J., Calvin, K., Daniel, J. S., Kainuma, M. L. T., Lamarque, J.-F., Matsumoto, K., Montzka, S. A., Raper, S. C. B., Riahi, K., Thomson, A., Velders, G. J. M., and van Vuuren, D. P.: The RCP greenhouse gas concentrations and their extensions from 1765 to 2300, *Climatic Change*, 109, 213–241, <https://doi.org/10.1007/s10584-011-0156-z>, 2011.
- 5 Millet, D. B., Baasandorj, M., Farmer, D. K., Thornton, J. A., Baumann, K., Brophy, P., Chaliyakunnel, S., Gouw, J. A. d., Graus, M., Hu, L., Koss, A., Lee, B. H., Lopez-Hilfiker, F. D., Neuman, J. A., Paulot, F., Peischl, J., Pollack, I. B., Ryerson, T. B., Warneke, C., Williams, B. J., and Xu, J.: A large and ubiquitous source of atmospheric formic acid, *Atmospheric Chemistry and Physics*, 15, 6283–6304, <https://doi.org/10.5194/acp-15-6283-2015>, <https://www.atmos-chem-phys.net/15/6283/2015/acp-15-6283-2015.pdf>, 2015.
- 10 Monks, S. A., Wilson, C., Emmons, L. K., Hannigan, J. W., Helmig, D., Blake, N. J., and Blake, D. R.: Using an Inverse Model to Reconcile Differences in Simulated and Observed Global Ethane Concentrations and Trends Between 2008 and 2014, *Journal of Geophysical Research: Atmospheres*, 123, 11,262–11,282, <https://doi.org/10.1029/2017JD028112>, <https://agupubs.onlinelibrary.wiley.com/doi/full/10.1029/2017JD028112>, 2018.
- 15 Morcrette, J., Boucher, O., Jones, L., Salmond, D., Bechtold, P., Beljaars, A., Benedetti, A., Bonet, A., Kaiser, J. W., Razinger, M., Schulz, M., Serrar, S., Simmons, A. J., Sofiev, M., Suttie, M., Tompkins, A. M., and Untch, A.: Aerosol analysis and forecast in the European Centre for Medium-Range Weather Forecasts Integrated Forecast System: Forward modeling, *Journal of Geophysical Research: Atmospheres*, 114, <https://doi.org/10.1029/2008JD011235>, <https://agupubs.onlinelibrary.wiley.com/doi/pdf/10.1029/2008JD011235>, 2009.
- Mungall, E. L., Abbatt, J. P. D., Wentzell, J. J. B., Wentworth, G. R., Murphy, J. G., Kunkel, D., Gute, E., Tarasick, D. W., Sharma, S., Cox, C. J., Uttal, T., and Liggio, J.: High gas-phase mixing ratios of formic and acetic acid in the High Arctic, *Atmospheric Chemistry and Physics*, 18, 10237–10254, <https://doi.org/10.5194/acp-18-10237-2018>, <https://www.atmos-chem-phys.net/18/10237/2018/acp-18-10237-2018.pdf>, 2018.
- 20 Neuman, J. A., Gao, R. S., Fahey, D. W., Holecek, J. C., Ridley, B. A., Walega, J. G., Grahek, F. E., Richard, E. C., McElroy, C. T., Thompson, T. L., Elkins, J. W., Moore, F. L., and Ray, E. A.: In situ measurements of HNO₃, NO_y, NO, and O₃ in the lower stratosphere and upper troposphere, *Atmospheric Environment*, 35, 5789–5797, [https://doi.org/10.1016/S1352-2310\(01\)00354-5](https://doi.org/10.1016/S1352-2310(01)00354-5), 2001.
- Nordeng, T. E.: Extended versions of the convective parametrization scheme at ECMWF and their impact on the mean and transient activity of the model in the tropics, 1994.
- 25 Pan, L. L., Honomichl, S. B., Kinnison, D. E., Abalos, M., Randel, W. J., Bergman, J. W., and Bian, J.: Transport of chemical tracers from the boundary layer to stratosphere associated with the dynamics of the Asian summer monsoon, *Journal of Geophysical Research: Atmospheres*, 121, 14,159–14,174, <https://doi.org/10.1002/2016JD025616>, <https://agupubs.onlinelibrary.wiley.com/doi/full/10.1002/2016JD025616>, 2016.
- 30 Park, M., Randel, W. J., Gettelman, A., Massie, S. T., and Jiang, J. H.: Transport above the Asian summer monsoon anticyclone inferred from Aura Microwave Limb Sounder tracers, *Journal of Geophysical Research*, 112, 253, <https://doi.org/10.1029/2006JD008294>, 2007.
- Park, M., Randel, W. J., Emmons, L. K., Bernath, P. F., Walker, K. A., and Boone, C. D.: Chemical isolation in the Asian monsoon anticyclone observed in Atmospheric Chemistry Experiment (ACE-FTS) data, *Atmospheric Chemistry and Physics*, 8, 757–764, <https://doi.org/10.5194/acp-8-757-2008>, 2008.
- 35 Paulot, F., Wunch, D., Crouse, J. D., Toon, G. C., Millet, D. B., DeCarlo, P. F., Vigouroux, C., Deutscher, N. M., González Abad, G., Notholt, J., Warneke, T., Hannigan, J. W., Warneke, C., Gouw, J. A. d., Dunlea, E. J., Mazière, M. D., Griffith, D. W. T., Bernath, P., Jimenez, J. L., and Wennberg, P. O.: Importance of secondary sources in the atmospheric budgets of formic and acetic acids, *Atmospheric Chemistry and Physics*, 11, 1989–2013, <https://doi.org/10.5194/acp-11-1989-2011>, <https://www.atmos-chem-phys.net/11/1989/2011/acp-11-1989-2011.pdf>, 2011.

- Pisso, I. and Legras, B.: Turbulent vertical diffusivity in the sub-tropical stratosphere, *Atmospheric Chemistry and Physics*, 8, 697–707, <https://doi.org/10.5194/acp-8-697-2008>, <https://www.atmos-chem-phys.net/8/697/2008/acp-8-697-2008.pdf>, 2008.
- Randel, W. J. and Jensen, E. J.: Physical processes in the tropical tropopause layer and their roles in a changing climate, *Nature Geoscience*, 6, 169–176, <https://doi.org/10.1038/ngeo1733>, <https://www.nature.com/articles/ngeo1733.pdf>, 2013.
- 5 Reiner, T., Möhler, O., and Arnold, F.: Measurements of acetone, acetic acid, and formic acid in the northern midlatitude upper troposphere and lower stratosphere, *Journal of Geophysical Research: Atmospheres*, 104, 13 943–13 952, <https://doi.org/10.1029/1999JD900030>, <https://agupubs.onlinelibrary.wiley.com/doi/full/10.1029/1999JD900030>, 1999.
- Riese, M., Oelhaf, H., Preusse, P., Blank, J., Ern, M., Friedl-Vallon, F., Fischer, H., Guggenmoser, T., Höpfner, M., Hoor, P., Kaufmann, M., Orphal, J., Plöger, F., Spang, R., Suminska-Ebersoldt, O., Ungerermann, J., Vogel, B., and Woiwode, W.: Gimballed Limb Observer for Radiance Imaging of the Atmosphere (GLORIA) scientific objectives, *Atmospheric Measurement Techniques*, 7, 1915–1928, <https://doi.org/10.5194/amt-7-1915-2014>, 2014.
- 10 Rinsland, C. P., Zander, R., Farmer, C. B., Norton, R. H., and Russell, J. M.: Concentrations of ethane (C₂H₆) in the lower stratosphere and upper troposphere and acetylene (C₂H₂) in the upper troposphere deduced from atmospheric trace molecule spectroscopy/Spacelab 3 spectra, *Journal of Geophysical Research: Atmospheres*, 92, 11 951–11 964, <https://doi.org/10.1029/JD092iD10p11951>, <https://agupubs.onlinelibrary.wiley.com/doi/full/10.1029/JD092iD10p11951>, 1987.
- 15 Rinsland, C. P., Dufour, G., Boone, C. D., Bernath, P. F., and Chiou, L.: Atmospheric Chemistry Experiment (ACE) measurements of elevated Southern Hemisphere upper tropospheric CO, C₂H₆, HCN, and C₂H₂ mixing ratios from biomass burning emissions and long-range transport, *Geophysical Research Letters*, 32, <https://doi.org/10.1029/2005GL024214>, <https://agupubs.onlinelibrary.wiley.com/doi/full/10.1029/2005GL024214>, 2005.
- 20 Rinsland, C. P., Boone, C. D., Bernath, P. F., Mahieu, E., Zander, R., Dufour, G., Clerbaux, C., Turquety, S., Chiou, L., McConnell, J. C., Neary, L., and Kaminski, J. W.: First space-based observations of formic acid (HCOOH): Atmospheric Chemistry Experiment austral spring 2004 and 2005 Southern Hemisphere tropical-mid-latitude upper tropospheric measurements, *Geophysical Research Letters*, 33, <https://doi.org/10.1029/2006GL027128>, <https://agupubs.onlinelibrary.wiley.com/doi/full/10.1029/2006GL027128>, 2006.
- 25 Roeckner, E., Brokopf, R., Esch, M., Giorgetta, M., Hagemann, S., Kornblüeh, L., Manzini, E., Schlese, U., and Schulzweida, U.: Sensitivity of Simulated Climate to Horizontal and Vertical Resolution in the ECHAM5 Atmosphere Model, *Journal of Climate*, 19, 3771–3791, <https://doi.org/10.1175/JCLI3824.1>, 2006.
- Safieddine, S., Boynard, A., Hao, N., Huang, F., Wang, L., Ji, D., Barret, B., Ghude, S. D., Coheur, P.-F., Hurtmans, D., and Clerbaux, C.: Tropospheric ozone variability during the East Asian summer monsoon as observed by satellite (IASI), aircraft (MOZAIC) and ground stations, *Atmospheric Chemistry and Physics*, 16, 10 489–10 500, <https://doi.org/10.5194/acp-16-10489-2016>, <https://www.atmos-chem-phys.net/16/10489/2016/acp-16-10489-2016.pdf>, 2016.
- 30 Sander, R., Baumgaertner, A., Gromov, S., Harder, H., Jöckel, P., Kerkweg, A., Kubistin, D., Regelin, E., Riede, H., Sandu, A., Taraborrelli, D., Tost, H., and Xie, Z.-Q.: The atmospheric chemistry box model CAABA/MECCA-3.0, *Geoscientific Model Development*, 4, 373–380, <https://doi.org/10.5194/gmd-4-373-2011>, <https://www.geosci-model-dev.net/4/373/2011/gmd-4-373-2011.pdf>, 2011.
- Santee, M. L., Lambert, A., Read, W. G., Livesey, N. J., Cofield, R. E., Cuddy, D. T., Daffer, W. H., Drouin, B. J., Froidevaux, L., Fuller, R. A., Jarnot, R. F., Knosp, B. W., Manney, G. L., Perun, V. S., Snyder, W. V., Stek, P. C., Thurstans, R. P., Wagner, P. A., Waters, J. W., Muscari, G., de Zafra, R. L., Dibb, J. E., Fahey, D. W., Popp, P. J., Marcy, T. P., Jucks, K. W., Toon, G. C., Stachnik, R. A., Bernath, P. F., Boone, C. D., Walker, K. A., Urban, J., and Murtagh, D.: Validation of the Aura Microwave Limb Sounder HNO₃ measurements, *Journal*

- of Geophysical Research: Atmospheres, 112, 2007JD008 721, <https://doi.org/10.1029/2007JD008721>, <http://onlinelibrary.wiley.com/doi/10.1029/2007JD008721/full>, 2007.
- Santee, M. L., Manney, G. L., Livesey, N. J., Froidevaux, L., Schwartz, M. J., and Read, W. G.: Trace gas evolution in the lowermost stratosphere from Aura Microwave Limb Sounder measurements, *Journal of Geophysical Research: Atmospheres*, 116, <https://doi.org/10.1029/2011JD015590>, <http://onlinelibrary.wiley.com/doi/10.1029/2011JD015590/full>, 2011.
- Santee, M. L., Manney, G. L., Livesey, N. J., Schwartz, M. J., Neu, J. L., and Read, W. G.: A comprehensive overview of the climatological composition of the Asian summer monsoon anticyclone based on 10 years of Aura Microwave Limb Sounder measurements, *Journal of Geophysical Research: Atmospheres*, 122, 5491–5514, <https://doi.org/10.1002/2016JD026408>, <http://onlinelibrary.wiley.com/doi/10.1002/2016JD026408/full>, 2017.
- 10 Schumann, U. and Huntrieser, H.: The global lightning-induced nitrogen oxides source, *Atmospheric Chemistry and Physics*, 7, 3823–3907, <https://doi.org/10.5194/acp-7-3823-2007>, 2007.
- Seinfeld, J. H. and Pandis, S. N.: *Atmospheric Chemistry and Physics: From Air Pollution to Climate Change*. John Wiley & Sons, Incorporated, New York, UNITED STATES, 2016.
- Sheese, P. E., Walker, K. A., Boone, C. D., McLinden, C. A., Bernath, P. F., Bourassa, A. E., Burrows, J. P., Degenstein, D. A., Funke, B., Fussen, D., Manney, G. L., McElroy, C. T., Murtagh, D., Randall, C. E., Raspollini, P., Rozanov, A., Russell III, J. M., Suzuki, M., Shiotani, M., Urban, J., Clarmann, T. V., and Zawodny, J. M.: Validation of ACE-FTS version 3.5 NO_y species profiles using correlative satellite measurements, *Atmospheric Measurement Techniques*, 9, 5781–5810, <https://doi.org/10.5194/amt-9-5781-2016>, <https://www.atmos-meas-tech.net/9/5781/2016/amt-9-5781-2016.pdf>, 2016.
- 15 Singh, H., Chen, Y., Tabazadeh, A., Fukui, Y., Bey, I., Yantosca, R., Jacob, D., Arnold, F., Wohlfrom, K., Atlas, E., Flocke, F., Blake, D., Blake, N., Heikes, B., Snow, J., Talbot, R., Gregory, G., Sachse, G., Vay, S., and Kondo, Y.: Distribution and fate of selected oxygenated organic species in the troposphere and lower stratosphere over the Atlantic, *Journal of Geophysical Research: Atmospheres*, 105, 3795–3805, <https://doi.org/10.1029/1999JD900779>, <https://agupubs.pericles-prod.literatumonline.com/doi/full/10.1029/1999JD900779>, 2000.
- 20 Singh, H., Chen, Y., Staudt, A., Jacob, D., Blake, D., Heikes, B., and Snow, J.: Evidence from the Pacific troposphere for large global sources of oxygenated organic compounds, *Nature*, 410, 1078, <https://doi.org/10.1038/35074067>, <https://www.nature.com/articles/35074067.pdf>, 2001.
- 25 Singh, H. B.: Reactive nitrogen in the troposphere, *Environmental science & technology*, 21, 320–327, 1987.
- Spang, R., Remedios, J. J., and Brarkley, M. P.: Colour indices for the detection and differentiation of cloud types in infra-red limb emission spectra, *Advances in Space Research*, 33, 1041–1047, [https://doi.org/10.1016/S0273-1177\(03\)00585-4](https://doi.org/10.1016/S0273-1177(03)00585-4), [/science/article/pii/S0273117703005854/pdf?md5=1e01c4a59e7a98f03118799b17f4e0a1&pid=1-s2.0-S0273117703005854-main.pdf](https://www.sciencedirect.com/science/article/pii/S0273117703005854/pdf?md5=1e01c4a59e7a98f03118799b17f4e0a1&pid=1-s2.0-S0273117703005854-main.pdf), 2004.
- 30 Stiller, G. P., ed.: *The Karlsruhe Optimized and Precise Radiative transfer Algorithm (KOPRA)*, vol. FZKA 6487 of *Wissenschaftliche Berichte*, Forschungszentrum Karlsruhe, 2000.
- Stohl, A., Forster, C., Frank, A., Seibert, P., and Wotawa, G.: Technical note: The Lagrangian particle dispersion model FLEXPART version 6.2, *Atmospheric Chemistry and Physics*, 5, 2461–2474, <https://doi.org/10.5194/acp-5-2461-2005>, <https://www.atmos-chem-phys.net/5/2461/2005/acp-5-2461-2005.pdf>, 2005.
- 35 Sèze, G., Pelon, J., Derrien, M., Le Gléau, H., and Six, B.: Evaluation against CALIPSO lidar observations of the multi-geostationary cloud cover and type dataset assembled in the framework of the Megha-Tropiques mission, *Quarterly Journal of the Royal Meteorological Society*, 141, 774–797, <https://doi.org/10.1002/qj.2392>, <https://rmets.onlinelibrary.wiley.com/doi/pdf/10.1002/qj.2392>, 2015.

- Tiedtke, M.: A Comprehensive Mass Flux Scheme for Cumulus Parameterization in Large-Scale Models, *Monthly Weather Review*, 117, 1779–1800, [https://doi.org/10.1175/1520-0493\(1989\)117<1779:ACMFSF>2.0.CO;2](https://doi.org/10.1175/1520-0493(1989)117<1779:ACMFSF>2.0.CO;2), <https://journals.ametsoc.org/mwr/article/117/8/1779/64184>, 1989.
- Tissier, A.-S. and Legras, B.: Convective sources of trajectories traversing the tropical tropopause layer, *Atmospheric Chemistry and Physics*, 16, 3383–3398, <https://doi.org/10.5194/acp-16-3383-2016>, <https://www.atmos-chem-phys.net/16/3383/2016/acp-16-3383-2016.pdf>, 2016.
- Tost, H., Jöckel, P., and Lelieveld, J.: Influence of different convection parameterisations in a GCM, *Atmospheric Chemistry and Physics*, 6, 5475–5493, <https://doi.org/10.5194/acp-6-5475-2006>, <https://acp.copernicus.org/articles/6/5475/2006/>, 2006.
- Ungermann, J., Pan, L. L., Kalicinsky, C., Olschewski, F., Knieling, P., Blank, J., Weigel, K., Guggenmoser, T., Strohm, F., Hoffmann, L., and Riese, M.: Filamentary structure in chemical tracer distributions near the subtropical jet following a wave breaking event, *Atmospheric Chemistry and Physics*, 13, 10517–10534, <https://doi.org/10.5194/acp-13-10517-2013>, <https://www.atmos-chem-phys.net/13/10517/2013/acp-13-10517-2013.pdf>, 2013.
- Ungermann, J., Ern, M., Kaufmann, M., Müller, R., Spang, R., Ploeger, F., Vogel, B., and Riese, M.: Observations of PAN and its confinement in the Asian summer monsoon anticyclone in high spatial resolution, *Atmospheric Chemistry and Physics*, 16, 8389–8403, <https://doi.org/10.5194/acp-16-8389-2016>, <http://www.atmos-chem-phys.net/16/8389/2016/acp-16-8389-2016.pdf>, 2016.
- Vogel, B., Günther, G., Müller, R., Groß, J.-U., and Riese, M.: Impact of different Asian source regions on the composition of the Asian monsoon anticyclone and of the extratropical lowermost stratosphere, *Atmospheric Chemistry and Physics*, 15, 13699–13716, <https://doi.org/10.5194/acp-15-13699-2015>, <http://www.atmos-chem-phys.net/15/13699/2015/acp-15-13699-2015.pdf>, 2015.
- Vogel, B., Günther, G., Müller, R., Groß, J.-U., Afchine, A., Bozem, H., Hoor, P., Krämer, M., Müller, S., Riese, M., Rolf, C., Spelten, N., Stiller, G. P., Ungermann, J., and Zahn, A.: Long-range transport pathways of tropospheric source gases originating in Asia into the northern lower stratosphere during the Asian monsoon season 2012, *Atmospheric Chemistry and Physics*, 16, 15301–15325, <https://doi.org/10.5194/acp-16-15301-2016>, <https://www.atmos-chem-phys.net/16/15301/2016/acp-16-15301-2016.pdf>, 2016.
- Vogel, B., Müller, R., Günther, G., Spang, R., Hanumanthu, S., Li, D., Riese, M., and Stiller, G. P.: Lagrangian simulations of the transport of young air masses to the top of the Asian monsoon anticyclone and into the tropical pipe, *Atmospheric Chemistry and Physics*, 19, 6007–6034, <https://doi.org/10.5194/acp-19-6007-2019>, <https://www.atmos-chem-phys.net/19/6007/2019/acp-19-6007-2019.pdf>, 2019.
- von Clarmann, T., Höpfner, M., Kellmann, S., Linden, A., Chauhan, S., Funke, B., Grabowski, U., Glatthor, N., Kiefer, M., Schieferdecker, T., Stiller, G. P., and Versick, S.: Retrieval of temperature, H₂O, O₃, HNO₃, CH₄, N₂O, ClONO₂ and ClO from MIPAS reduced resolution nominal mode limb emission measurements, *Atmospheric Measurement Techniques*, 2009.
- Wang, Y., Ma, Y.-F., Eskes, H., Inness, A., Flemming, J., and Brasseur, G. P.: Evaluation of the CAMS global atmospheric trace gas reanalysis 2003–2016 using aircraft campaign observations, *Atmospheric Chemistry and Physics*, 20, 4493–4521, <https://doi.org/10.5194/acp-20-4493-2020>, 2020.
- Wiegele, A., Glatthor, N., Höpfner, M., Grabowski, U., Kellmann, S., Linden, A., Stiller, G., and von Clarmann, T.: Global distributions of C₂H₆, C₂H₂, HCN, and PAN retrieved from MIPAS reduced spectral resolution measurements, *Atmospheric Measurement Techniques*, 5, 723–734, <https://doi.org/10.5194/amt-5-723-2012>, <https://www.atmos-meas-tech.net/5/723/2012/amt-5-723-2012.pdf>, 2012.
- WMO, ed.: Scientific Assessment of Ozone Depletion: 2018, vol. 58 of *Report / World Meteorological Organization, Global Ozone Research and Monitoring Project*, WMO, Geneva, Switzerland, <https://www.esrl.noaa.gov/csd/assessments/ozone/2018/report/2018OzoneAssessment.pdf>, 2019.

- Wohlmann, I. and Rex, M.: The Lagrangian chemistry and transport model ATLAS: Validation of advective transport and mixing, *Geoscientific Model Development*, 2, 153–173, <https://doi.org/10.5194/gmd-2-153-2009>, <https://www.geosci-model-dev.net/2/153/2009/gmd-2-153-2009.pdf>, 2009.
- Wohlmann, I., Lehmann, R., Gottwald, G. A., Peters, K., Protat, A., Louf, V., Williams, C., Feng, W., and Rex, M.: A Lagrangian convective
5 transport scheme including a simulation of the time air parcels spend in updrafts (LaConTra v1.0), *Geoscientific Model Development*,
12, 4387–4407, <https://doi.org/10.5194/gmd-12-4387-2019>, <https://gmd.copernicus.org/articles/12/4387/2019/gmd-12-4387-2019.html>,
2019.
- Woiwode, W., Oelhaf, H., Gulde, T., Piesch, C., Maucher, G., Ebersoldt, A., Keim, C., Höpfner, M., Khaykin, S., Ravegnani, F., Ulanovsky,
A. E., Volk, C. M., Hösen, E., Dörnbrack, A., Ungermann, J., Kalicinsky, C., and Orphal, J.: MIPAS-STR measurements in the Arctic
10 UTLS in winter/spring 2010: Instrument characterization, retrieval and validation, *Atmospheric Measurement Techniques*, 5, 1205–1228,
<https://doi.org/10.5194/amt-5-1205-2012>, 2012.
- Wolff, M. A., Kerzenmacher, T., Strong, K., Walker, K. A., Toohey, M., Dupuy, E., Bernath, P. F., Boone, C. D., Brohede, S., Catoire, V., von
Clarmann, T., Coffey, M., Daffer, W. H., Mazière, M. D., Duchatelet, P., Glatthor, N., Griffith, D. W. T., Hannigan, J., Hase, F., Höpfner,
M., Huret, N., Jones, N., Jucks, K., Kagawa, A., Kasai, Y., Kramer, I., Küllmann, H., Kuttippurath, J., Mahieu, E., Manney, G., McElroy,
15 C. T., McLinden, C., Mébarki, Y., Mikuteit, S., Murtagh, D., Piccolo, C., Raspollini, P., Ridolfi, M., Ruhnke, R., Santee, M., Senten, C.,
Smale, D., Tétard, C., Urban, J., and Wood, S.: Validation of HNO₃, ClONO₂, and N₂O₅ from the Atmospheric Chemistry Experiment
Fourier Transform Spectrometer (ACE-FTS), *Atmospheric Chemistry and Physics*, 8, 3529–3562, <https://doi.org/10.5194/acp-8-3529-2008>,
<https://www.atmos-chem-phys.net/8/3529/2008/acp-8-3529-2008.pdf>, 2008.
- Xiao, Y., Jacob, D. J., and Turquety, S.: Atmospheric acetylene and its relationship with CO as an indicator of air mass age, *Journal of Geo-
20 physical Research: Atmospheres*, 112, <https://doi.org/10.1029/2006JD008268>, <https://agupubs.onlinelibrary.wiley.com/doi/full/10.1029/2006JD008268>, 2007.
- Zahn, A., Weppner, J., Widmann, H., Schlote-Holubek, K., Burger, B., Kühner, T., and Franke, H.: A fast and precise chemiluminescence
ozone detector for eddy flux and airborne application, *Atmospheric Measurement Techniques*, 5, 363–375, <https://doi.org/10.5194/amt-5-363-2012>,
<https://www.atmos-meas-tech.net/5/363/2012/amt-5-363-2012.pdf>, 2012.